Title: Early adaptation in a microbial community is dominated by mutualism-enhancing mutations

Authors: Sandeep Venkataram[1], Huan-Yu Kuo[1,2], Erik F. Y. Hom[3], Sergey Kryazhimskiy[1,*]

Affiliations:

[1]Division of Biological Sciences, University of California San Diego, La Jolla, CA 92093;

[2]Department of Physics, University of California San Diego, La Jolla, CA 92093;

[3]Department of Biology and Center for Biodiversity and Conservation Research, University of Mississippi, University, MS 38677

[*]Corresponding author: skryazhi@ucsd.edu

Abstract: Evolutionary dynamics in ecological communities are often repeatable, but how species interactions affect the distribution of evolutionary outcomes at different levels of biological organization is unclear. Here, we use barcode lineage tracking to experimentally address this gap in a facultatively mutualistic community formed by the alga *Chlamydomonas reinhardtii* and the yeast *Saccharomyces cerevisiae*. We find that interactions with the alga alter the magnitude but not the sign of the fitness effects of adaptive mutations in yeast, changing the distribution of mutants contending for fixation. In the presence of alga, most contending mutants reinforce the mutualism and make evolution more repeatable at the community level. Thus, ecological interactions not only alter the trajectory of evolution but also dictate its repeatability at multiple levels of biological organization.

One-sentence summary: The mutualistic interaction between two species drives evolution to increase both species' yields.

Multispecies communities in similar environments often evolve repeatably toward similar ecological states (*1–6*). A significant degree of repeatability in eco-evolutionary dynamics is expected when selection is driven by the same abiotic environment and when it acts upon standing genetic variation (*7*, *8*). In contrast, new mutations and/or selection driven by species interactions can increase the role of priority effects, epistasis and coevolution, which may steer the eco-evolutionary dynamics towards new states and reduce its repeatability (*8–11*). However, repeatability even in this regime is surprisingly high (*12–22*), suggesting that eco-evolutionary dynamics are subject to additional poorly understood constraints.

Evolution experiments of microbial monocultures have shown that the genetic architecture of organisms constrains the distribution of evolutionary outcomes for traits at higher levels of biological organization (*23*, *24*), so that evolution at these levels is highly repeatable (*25*, *26*). In multispecies communities, however, the distribution of eco-evolutionary outcomes depends not only on the genetic architecture of community members but also on the ecological interactions between them. Interactions can steer community evolution towards novel ecological states (*14*, *19*, *27*) and influence its repeatability (*17*, *28–31*). However, how ecological interactions alter the underlying distribution of eco-evolutionary outcomes at various levels of organization, to our knowledge, has never been directly measured. We set out to address this gap in an experimental microbial community for which there is no prior expectation about how ecological interactions would affect the eco-evolutionary dynamics.

This community consists of two microbes, the yeast *Saccharomyces cerevisiae* and the alga *Chlamydomonas reinhardtii* (*32*). We propagate them over multiple cycles of growth and dilution in well-mixed and well-lit conditions (*SM*). In these conditions, both species reproduce asexually and interact via competition and nutrient exchange, forming a facultative mutualism in a medium containing ammonia and nitrite as potential sources of nitrogen, as well as glucose and CO_2 as potential sources of carbon (*30*; *SM*). Yeast growth is inhibited by algae at the beginning of each cycle, likely due to competition for the initial supply of ammonia (Figure S1; *SM*). Once this supply is exhausted, the alga switches to metabolizing nitrite (which cannot be metabolized by yeast) and excretes ammonia, thereby supporting yeast survival while also benefiting from additional dissolved CO_2 produced by the yeast (Figure S1) (*32*). There is no clear *a priori* expectation that this community would repeatably evolve towards certain ecological states. For example, yeast could adapt by improving its competitive ability (e.g. by increasing the rate of ammonia consumption), potentially driving the alga to extinction, or by improving its cooperation (e.g. by limiting its ammonia uptake early in the growth cycle to receive a fitness benefit later in the cycle) and thereby strengthen the mutualism.

Using this community, we aim to tease apart how ecological interactions affect the distribution of eco-evolutionary outcomes. This distribution can change over time because of epistasis within each species (*33*) and coevolution between species (*19*, *34*). To avoid these complications, we characterize single adaptive mutations rather than multi-step eco-evolutionary trajectories, capturing adaptive mutants before any of them reach high enough frequencies to significantly modify the environment. We focus on adaptive mutations available to one community member, the yeast, because it is more likely to acquire the first adaptive mutations in our community (see *SM*). To this end, we leverage barcode lineage tracking (BLT) technology (*35*, *36*) to sample adaptive mutations in yeast. We examine how ecological interactions affect the diversity of these mutations at the genetic, phenotypic, fitness and community levels by comparing mutations that

arise in yeast evolving in co-culture with alga ("C-condition") versus those that arise in yeast evolving alone ("A-condition").

We first asked whether and how ecological interactions with algae change the diversity of adaptive mutations available to yeast in terms of genotype and fitness. We carried out five replicate BLT experiments in yeast in A- and C-conditions (*SM*). In each population, we tracked the frequencies of about 5×10^5 neutral DNA barcodes integrated into the yeast genome (*37*) over 17 growth and dilution cycles. We identified a total of 14,098 and 14,523 adapted lineages across all replicates in the A- and C-conditions, respectively (*SM;* Figures S2–S5). The similarity of these numbers suggests that the presence of algae does not dramatically change the rate at which beneficial mutations arise in yeast.

Each adapted lineage is expected to initially carry a single driver mutation (*35*), which allows us to estimate the competitive fitness effects of these mutations from barcode frequency trajectories (*SM*). The resulting distributions of fitness effects of beneficial mutations (bDFEs) are much broader than would be expected from measurement noise alone in both conditions (*SM*), indicating that yeast has access to multiple adaptive mutations with different fitness effects. Furthermore, the bDFEs in A- and C-conditions are different (Figures 1A). Specifically, ecological interactions with algae reduce the bDFE median (1.60 in A vs. 1.50 in C; $P < 10^{-4}$, permutation test) but increase the width of the distribution (interquartile range (IQR) = 0.31 in A vs. IQR = 0.37 in C; $P < 10^{-4}$, permutation test). This increase in width is associated with the appearance of two peaks with higher relative fitness values around 2.0 and 2.5 (Figure 1A).

We then asked whether interactions with algae alter only the fitness effects of beneficial mutations available to yeast or also change which mutations are beneficial. In other words, do some mutations that are beneficial in the A-condition become deleterious in the C-condition and/or vice versa? We randomly sampled 219 yeast clones from distinct adapted lineages in the A-condition ("A-mutants") and 189 yeast clones from distinct adapted lineages in the C-condition ("C-mutants"). Clones were sampled at cycle nine where we expect that most adapted lineages are still driven by single beneficial mutations. We used competition assays to measure the fitness of all A- and C-mutants in both A- and C-conditions relative to the ancestor (*SM*; Figures S6–S8; Data S1). These direct fitness estimates are concordant with the estimates from the BLT experiment (see *SM*; Figure S9). We find that the C-mutants have significantly higher fitness in their "home" C-condition than the A-mutants ($P = 5\times10^{-5}$, t-test) and the A-mutants are more fit in the A-condition than the C-mutants ($P = 7\times10^{-5}$), consistent with a signature of local adaptation. Interactions with algae significantly alter the fitness of 43% (178/410) of A- and C-mutants. However, fitness is positively correlated between the two conditions for all mutants (Figure 1B; $R = 0.70$, $P < 10^{-10}$) and crucially, none of the A- or C-mutants are deleterious in their "non-home" condition. Therefore, the presence of algae changes the fitness benefits provided by adaptive mutations, but does not measurably alter which mutations are beneficial.

Given that all sampled mutants remain beneficial in the presence and absence of algae and mutant fitness is correlated between the two treatments, we expect that the set of A-mutants would be genetically indistinguishable from the set of C-mutants. To test this expectation, we sequenced the genomes of 181 out of 189 C-mutants, 215 out of 221 A-mutants, as well as eight evolved neutral and 24 ancestral isolates as controls (*SM*; Figures S10–S13; Data S2). We found 176 large chromosomal duplications and deletions across 14 loci in the genomes of A- and C-mutants and none in the ancestral or neutral isolates. All of these large mutations are likely adaptive (see *SM*), with a typical A- and C-mutant carrying 0.39 and 0.51 of them, respectively.

We also discovered 185 small indels and point mutations at 63 loci where mutations are found in A- and C-mutants more often than expected by chance (see *SM*), suggesting that these small mutations are also adaptive. A typical A- and C-mutant carries 0.35 and 0.60 of them, respectively. Overall, we identified 361 beneficial mutations across 77 loci in 250 out of 396 adapted mutants, with each A- and C-mutant carrying on average 0.74 and 1.11 such mutations, respectively (Table S1, Data S2).

We measured the diversity of adaptive mutations carried by A- and C-mutants using the probability of genetic parallelism, P_g, i.e., the probability that two random clones share a mutation at the same driver locus, so that lower P_g values imply higher diversity. We find that the diversity is high in both A- and C-mutants (P_g = 6.0% and 8.5%, respectively), but there is no statistically significant difference (see *SM*). Nevertheless, there are large differences in the frequency distribution of driver mutations among A- and C-mutants (Figures 1C and S14, Data S3; $P = 5\times10^{-8}$, χ^2-test), suggesting that the chances for the same beneficial mutation to rise to high enough frequency and be sampled are markedly different between the A- and C-conditions. The starkest difference is observed for chromosome XIV: 10% (18/181) of C-mutants carry a whole chromosome amplification but none of the 215 A-mutants do (Figures 1C and S14), despite chrXIV-3n mutations being beneficial in both conditions (Figure 1B).

This unexpected observation can be explained by the dynamics of rapid adaptation in populations with limited recombination. In such populations, clonal interference can prevent weak or rare beneficial mutations from reaching even moderately high frequencies (*38*, *39*). Therefore, the same beneficial mutation can have dramatically different chances of being sampled in the two conditions if it is located in different parts of the respective bDFEs. Consistent with this explanation, a typical chrXIV-3n mutant is 2.05 times more fit per cycle than the ancestor and ranks in the top 11% of most fit mutants in the C-condition, while being only 1.59 times more fit than the ancestor and ranking in the 53rd percentile in the A-condition (Figure 1C). Other mutations with strong discrepancies in their representation among A- and C-mutants show similar shifts in their fitness effects and rank (Figure 1C, Data S3). In general, interactions with algae shift the fitness ranks of mutants between conditions by 14% on average. We used evolutionary simulations to confirm that these differences are sufficient to explain the observed genetic differences between A- and C-mutants (see *SM*; Figures S15, S16, Table S2).

Mutations that are more likely to be in our sample also have higher chances of winning the clonal competition, i.e., they are contending for fixation. Thus, our results imply that the presence of alga does not change the sign of fitness effects of mutations, but nevertheless markedly shifts which mutations contend for fixation. We wondered what ecological consequences these mutations would have if they actually spread and fixed in the yeast population. In a mutualistic community, adaptive mutations may alter public-good production in a way that either enhances or weakens the mutualism (*40*, *41*). In our community, yeast and algae both compete and cooperate, so that mutations ranging from mutualism-weakening to mutualism-enhancing could conceivably be beneficial to yeast. However, it is unclear how commonly mutations with different ecological effects contribute to adaptation and whether the presence of alga shifts these contributions relative to the abiotic condition. To address these questions, we selected 28 C-mutants and 31 A-mutants that span the diversity of contending mutations (*SM*). We then quantified their impact on the strength of mutualism by growing each mutant in coculture with the ancestral alga strain (i.e., forming “mutant communities”) and measuring the relative “yields” of both species, defined as their densities at the end of the 5-day

growth cycle. We report these yields as the percent change in final density relative to the ancestral community (*SM*, Figure S17).

We find that yeast and alga yields are positively correlated (Figure 2A), as may be expected for a mutualism. 14% (8/59) of tested adaptive mutants significantly decrease the yield of at least one of the species, while 47% (28/59) of mutants significantly increase it. The median change in yield is +63% for yeast (IQR = [+4%, +170%]) and +47% for alga (IQR = [+1%, +113%]), with some mutations decreasing the yield by as much as 58% and others increasing it by as much as as 265% (Figure 2A). Thus, the ecological consequences of the first adaptive step in yeast are highly diverse across both A- and C-mutants, with a trend towards stronger mutualism (as quantified by species yields).

While evolution of monocultures typically does not lead to higher yields (*42*), we observed that contending yeast mutants in our experiment typically increase the yields of both species, suggesting a positive correlation between competitive fitness and yield. While we indeed observe such correlations in both conditions, they are strong in the C-condition (Figures 2B and S18) but weak in the A-condition (Figures 2C and S18). Consistent with this observation, the yields of yeast and alga in C-mutant communities are on average higher by 103% ($P = 3\times10^{-4}$, permutation t-test) and 57% ($P = 0.004$) than those in the A-mutant communities, which themselves are higher by 37% ($P = 0.02$) and 28% ($P = 0.03$) than those of the ancestral community. The yield differences between A- and C-mutant communities remain large and significant after accounting for the frequency with which different driver mutations are observed ($P < 2\times10^{-5}$, weighted t-test, Figure S19).

The presence of alga may also affect the repeatability of evolution at the community level. We measure such repeatability by the probability of ecological parallelism P_e, i.e., the probability that two random mutant communities have the same sign change (relative to the ancestral community) in yeast yield and the same sign change in alga yield. $P_e = 33.5\%$ for the A-mutant communities, compared to the null expectation of 25%, indicating that evolution in the A-condition would be only slightly more repeatable at the community level than expected by chance. In contrast, $P_e = 77\%$ for C-mutant communities, indicating that by shifting selection towards mutualism-enhancing mutants, the interactions with alga make community evolution much more repeatable at the ecological level ($P = 0.006$, permutation and resampling, see *SM*).

Does selection in the presence of alga favor increased cooperation in yeast directly or is cooperation a byproduct of selection for another trait (*22*, *43*)? Natural selection can directly favor rare mutualism-enhancing (more cooperative) yeast mutants only if such mutants preferentially receive fitness benefits from their alga partners (*44*). Our system is well-mixed, so that all diffusible benefits are shared by the entire culture, eliminating any potential fitness advantage of a rare mutualism-enhancing mutant (*22*, *45*). The only way to prevent such diffusion and ensure preferential benefit exchange with an alga partner is for such a mutant to form a physical association with the partner (*20*). However, we found no evidence for such associations (Figure S20; *SM*). Therefore, the increased cooperation of C-mutants is likely a byproduct (pleiotropic effect) of selection for one or more other traits.

We sought to identify traits under selection in the C-condition that could cause yields to increase. Both competitive fitness and yield depend on fundamental physiological and life-history traits embodied by yeast and algae, such as their growth rates, mortalities, nutrient consumption efficiencies, etc (*42*). Since measuring all potentially relevant traits was not feasible in this study,

we focused on two key traits that are known to be under selection in environments with variable nutrient availability. The maximum population growth rate, r, is important for competitive fitness when resources are abundant (*46*, *47*), particularly in the initial phase of each growth cycle. The carrying capacity, K, is an indicator of nutrient utilization efficiency, which is important for competitive fitness when resources are scarce (*46*, *47*), particularly in the later phase of each growth cycle. We estimated these two traits for all 59 mutants from monoculture growth-curve measurements (Figures S21, S22; *SM*), reasoning that these intrinsic traits would be relevant in both A- and C-conditions.

We observe that the sampled adaptive mutations have diverse effects on r and K. 32% (19/59) and 36% (21/59) of mutants have significantly higher and lower r than the ancestor, respectively, with the median change in r being –0.4% (IQR = [–12%, +7%]). At the same time, 31% (18/59) and 7% (4/59) of mutants reach either significantly higher or lower K than the ancestor, respectively, with the median change in K being +7% (IQR = [–2%, +16%]). Consistent with other systems (*48–50*), we observe a trade-off between the effects of mutations on r and K (Figure 3A).

To test whether r and K are under selection, we examined the correlation between these traits and competitive fitness among all 59 assayed mutants. We find weak or no correlation between either r or K and fitness in the A-condition (Figure S23A, B). As a result, the A-mutants have r and K values indistinguishable from the ancestor (average $\Delta r = +2\%$, $P = 0.27$; average $\Delta K = +3\%$; $P = 0.29$; permutation t-test). In contrast, fitness in the C-condition is positively correlated with K (Figure 3B, $R = 0.51$, $P < 10^{-4}$) and negatively correlated with r (Figure S23C, $R = -0.50$, $P < 10^{-4}$), consistent with the observed r vs K trade-off. C-mutants reach K values on average 16% higher than the ancestor ($P = 4\times10^{-4}$, permutation t-test) and 13% higher than A-mutants ($P = 0.04$). C-mutants also have a significantly lower r than both the ancestor (average $\Delta r = -15\%$, $P = 0.001$) and A-mutants ($\Delta r = -17\%$, $P = 7\times10^{-4}$). We infer that there is no detectable selection on r and K in the absence of alga, while the presence of alga induces selection that favors yeast mutants with lower r and higher K. This shift in selection increases the probability of phenotypic parallelism (defined analogously to P_e; *SM*) from 31.2% for the A-mutants to 43.5% for the C-mutants, but this increase is not statistically significant ($P = 0.21$, *SM*).

Finally, as expected, we find a significant positive correlation between the effects of mutations on K and the yields of both species in mutant communities (Figures 3C and S23D). Taken together, our observations suggest a plausible model for how adaptive evolution can favor mutualism enhancement in the absence of partner-fidelity feedbacks: ecological interactions with algae intensify selection for yeast mutants that use resources more efficiently (i.e., those that reach higher K), and once these mutants spread in the yeast population, they support higher yields of both members of the community. Whether mutualistic partners generally induce selection for lower r and/or higher K and whether such selection consistently leads to increased yields of both species remains to be determined.

The biochemical and cellular mechanisms by which the observed mutations enhance the mutualism are currently unknown. ChrXIV-3n amplifications are sometimes adaptive under ammonium limitation, possibly driven by the copy number of the gene *MEP2* that encodes a high affinity ammonium transporter (*51*). These adaptations are particularly beneficial to yeast in the C-condition, possibly because the alga provides a continuous but low flux of ammonia. ChrIV-1n mutations could be driven by the loss of the gene SIR4, which regulates chromatin silencing (*52*) and has been previously implicated in adaptation in yeast (*53*). Mutations in genes *HEM1*,

HEM2 and *HEM3* provide much larger fitness benefits in the C-condition compared to the A-condition (Data S3) possibly because they shift the metabolic balance towards fermentation at higher concentrations of dissolved oxygen produced by the alga (see *SM*). Elucidating these and other mechanisms of physiological adaptation may help us understand how and why microbial mutualists modify the environment to favor stronger mutualism and apparently improve coexistence (*54*, *55*) even in the absence of partner-fidelity feedbacks.

Overall, our results suggest that similar to abiotic conditions (*53*, *56*, *57*) microbial adaptation in the community context is driven by many mutations that are genetically and phenotypically diverse. Ecological interactions may not open up or close down any major adaptive paths; nevertheless, by altering the benefits of mutations and their rank order, interactions may canalize evolutionary trajectories at the community level. Thus, our results support the view (*58*) that despite the daunting complexity at the genetic level, evolution at the community level may be relatively simple and repeatable.

References

1. J. B. Losos, T. R. Jackman, A. Larson, K. Queiroz, L. Rodriguez-Schettino, Contingency and determinism in replicated adaptive radiations of island lizards. *Science*. **279**, 2115–2118 (1998).

2. R. Gillespie, Community assembly through adaptive radiation in Hawaiian spiders. *Science*. **303**, 356–359 (2004).

3. F. T. Burbrink, X. Chen, E. A. Myers, M. C. Brandley, R. A. Pyron, Evidence for determinism in species diversification and contingency in phenotypic evolution during adaptive radiation. *Proc. Biol. Sci.* **279**, 4817–4826 (2012).

4. E. D. Brodie 3rd, C. R. Feldman, C. T. Hanifin, J. E. Motychak, D. G. Mulcahy, B. L. Williams, E. D. Brodie Jr, Parallel arms races between garter snakes and newts involving tetrodotoxin as the phenotypic interface of coevolution. *J. Chem. Ecol.* **31**, 343–356 (2005).

5. M. Muschick, A. Indermaur, W. Salzburger, Convergent evolution within an adaptive radiation of cichlid fishes. *Curr. Biol.* **22**, 2362–2368 (2012).

6. H. D. Rundle, L. Nagel, J. Wenrick Boughman, D. Schluter, Natural selection and parallel speciation in sympatric sticklebacks. *Science*. **287**, 306–308 (2000).

7. R. D. H. Barrett, D. Schluter, Adaptation from standing genetic variation. *Trends Ecol. Evol.* **23**, 38–44 (2008).

8. T. Fukami, Historical contingency in community assembly: integrating niches, species pools, and priority effects. *Annu. Rev. Ecol. Evol. Syst.* **46**, 1–23 (2015).

9. O. Seehausen, Chance, historical contingency and ecological determinism jointly determine the rate of adaptive radiation. *Heredity* . **99**, 361–363 (2007).

10. J. B. Losos, Convergence, adaptation, and constraint. *Evolution*. **65**, 1827–1840 (2011).

11. Z. D. Blount, R. E. Lenski, J. B. Losos, Contingency and determinism in evolution: Replaying life's tape. *Science*. **362** (2018), doi:10.1126/science.aam5979.

12. P. B. Rainey, M. Travisano, Adaptive radiation in a heterogeneous environment. *Nature*. **394**, 69–72 (1998).

13. K. L. Hillesland, D. A. Stahl, Rapid evolution of stability and productivity at the origin of a microbial mutualism. *Proc. Natl. Acad. Sci. U. S. A.* **107**, 2124–2129 (2010).

14. D. Lawrence, F. Fiegna, V. Behrends, J. G. Bundy, A. B. Phillimore, T. Bell, T. G. Barraclough, Species interactions alter evolutionary responses to a novel environment. *PLoS Biol.* **10**, e1001330 (2012).

15. J. R. Meyer, D. T. Dobias, J. S. Weitz, J. E. Barrick, R. T. Quick, R. E. Lenski, Repeatability and contingency in the evolution of a key innovation in phage lambda. *Science*. **335**, 428–432 (2012).

16. M. D. Herron, M. Doebeli, Parallel evolutionary dynamics of adaptive diversification in *Escherichia coli*. *PLoS Biol.* **11**, e1001490 (2013).

17. H. Celiker, J. Gore, Clustering in community structure across replicate ecosystems following a long-term bacterial evolution experiment. *Nat. Commun.* **5**, 4643 (2014).

18. K. L. Hillesland, S. Lim, J. J. Flowers, S. Turkarslan, N. Pinel, G. M. Zane, N. Elliott, Y. Qin, L. Wu, N. S. Baliga, J. Zhou, J. D. Wall, D. A. Stahl, Erosion of functional independence early in the evolution of a microbial mutualism. *Proc. Natl. Acad. Sci. U. S. A.* **111**, 14822–14827 (2014).

19. W. R. Harcombe, J. M. Chacón, E. M. Adamowicz, L. M. Chubiz, C. J. Marx, Evolution of bidirectional costly mutualism from byproduct consumption. *Proc. Natl. Acad. Sci. U. S. A.* **115**, 12000–12004 (2018).

20. D. Preussger, S. Giri, L. K. Muhsal, L. Oña, C. Kost, Reciprocal fitness feedbacks promote the evolution of mutualistic cooperation. *Curr. Biol.* **30**, 3580–3590.e7 (2020).

21. N. Meroz, N. Tovi, Y. Sorokin, J. Friedman, Community composition of microbial microcosms follows simple assembly rules at evolutionary timescales. *Nat. Commun.* **12**, 2891 (2021).

22. S. F. M. Hart, C.-C. Chen, W. Shou, Pleiotropic mutations can rapidly evolve to directly benefit self and cooperative partner despite unfavorable conditions. *Elife*. **10** (2021), doi:10.7554/eLife.57838.

23. O. Tenaillon, A. Rodríguez-Verdugo, R. L. Gaut, P. McDonald, A. F. Bennett, A. D. Long, B. S. Gaut, The molecular diversity of adaptive convergence. *Science*. **335**, 457–461 (2012).

24. G. Kinsler, K. Geiler-Samerotte, D. A. Petrov, Fitness variation across subtle environmental perturbations reveals local modularity and global pleiotropy of adaptation. *Elife*. **9** (2020), doi:10.7554/eLife.61271.

25. M. J. Wiser, N. Ribeck, R. E. Lenski, Long-term dynamics of adaptation in asexual populations. *Science*. **342**, 1364–1367 (2013).

26. S. Kryazhimskiy, D. P. Rice, E. R. Jerison, M. M. Desai, Global epistasis makes adaptation predictable despite sequence-level stochasticity. *Science*. **344**, 1519–1522 (2014).

27. J. R. Meyer, D. T. Dobias, S. J. Medina, L. Servilio, A. Gupta, R. E. Lenski, Ecological speciation of bacteriophage lambda in allopatry and sympatry. *Science*. **354**, 1301–1304 (2016).

28. J. P. J. Hall, E. Harrison, M. A. Brockhurst, Competitive species interactions constrain abiotic

adaptation in a bacterial soil community. *Evol Lett*. **2**, 580–589 (2018).

29. M. Baumgartner, F. Bayer, K. R. Pfrunder-Cardozo, A. Buckling, A. R. Hall, Resident microbial communities inhibit growth and antibiotic-resistance evolution of *Escherichia coli* in human gut microbiome samples. *PLoS Biol.* **18**, e3000465 (2020).

30. T. Scheuerl, M. Hopkins, R. W. Nowell, D. W. Rivett, T. G. Barraclough, T. Bell, Bacterial adaptation is constrained in complex communities. *Nat. Commun.* **11**, 754 (2020).

31. E. M. Adamowicz, M. Muza, J. M. Chacón, W. R. Harcombe, Cross-feeding modulates the rate and mechanism of antibiotic resistance evolution in a model microbial community of *Escherichia coli* and *Salmonella enterica*. *PLoS Pathog.* **16**, e1008700 (2020).

32. E. F. Y. Hom, A. W. Murray, Niche engineering demonstrates a latent capacity for fungal-algal mutualism. *Science*. **345**, 94–98 (2014).

33. J. A. G. M. de Visser, J. Krug, Empirical fitness landscapes and the predictability of evolution. *Nat. Rev. Genet.* **15**, 480–490 (2014).

34. R. R. Nair, M. Vasse, S. Wielgoss, L. Sun, Y.-T. N. Yu, G. J. Velicer, Bacterial predator-prey coevolution accelerates genome evolution and selects on virulence-associated prey defences. *Nat. Commun.* **10**, 4301 (2019).

35. S. F. Levy, J. R. Blundell, S. Venkataram, D. A. Petrov, D. S. Fisher, G. Sherlock, Quantitative evolutionary dynamics using high-resolution lineage tracking. *Nature*. **519**, 181–186 (2015).

36. S. Venkataram, B. Dunn, Y. Li, A. Agarwala, J. Chang, E. R. Ebel, K. Geiler-Samerotte, L. Hérissant, J. R. Blundell, S. F. Levy, D. S. Fisher, G. Sherlock, D. A. Petrov, Development of a comprehensive genotype-to-fitness map of adaptation-driving mutations in yeast. *Cell*. **166**, 1585–1596.e22 (2016).

37. S. Boyer, L. Hérissant, G. Sherlock, Adaptation is influenced by the complexity of environmental change during evolution in a dynamic environment. *PLoS Genet.* **17**, e1009314 (2021).

38. S. Schiffels, G. J. Szöllosi, V. Mustonen, M. Lässig, Emergent neutrality in adaptive asexual evolution. *Genetics*. **189**, 1361–1375 (2011).

39. S. Venkataram, R. Monasky, S. H. Sikaroodi, S. Kryazhimskiy, B. Kacar, Evolutionary stalling and a limit on the power of natural selection to improve a cellular module. *Proceedings of the National Academy of Sciences*. **117**, 18582–18590 (2020).

40. J. L. Sachs, E. L. Simms, Pathways to mutualism breakdown. *Trends Ecol. Evol.* **21**, 585–592 (2006).

41. M. E. Frederickson, Rethinking mutualism stability: cheaters and the evolution of sanctions. *Q. Rev. Biol.* **88**, 269–295 (2013).

42. F. Vasi, M. Travisano, R. E. Lenski, Long-term experimental evolution in *Escherichia coli*. II. Changes in life-history traits during adaptation to a seasonal environment. *Am. Nat.* **144**, 432–456 (1994).

43. K. R. Foster, G. Shaulsky, J. E. Strassmann, D. C. Queller, C. R. L. Thompson, Pleiotropy as a mechanism to stabilize cooperation. *Nature*. **431**, 693–696 (2004).

44. J. L. Sachs, U. G. Mueller, T. P. Wilcox, J. J. Bull, The evolution of cooperation. *Q. Rev. Biol.* **79**, 135–160 (2004).

45. W. Harcombe, Novel cooperation experimentally evolved between species. *Evolution*. **64**, 2166–2172 (2010).

46. R. H. MacArthur, E. O. Wilson, *The theory of island biogeography* (Princeton University Press, Princeton, NJ, 2001), *Princeton Landmarks in Biology*.

47. D. Reznick, M. J. Bryant, F. Bashey, *r*- and *K*-selection revisited: the role of population regulation in life-history evolution. *Ecology*. **83**, 1509–1520 (2002).

48. L. D. Mueller, F. J. Ayala, Trade-off between r-selection and K-selection in Drosophila populations. *Proc. Natl. Acad. Sci. U. S. A.* **78**, 1303–1305 (1981).

49. M. Novak, T. Pfeiffer, R. E. Lenski, U. Sauer, S. Bonhoeffer, Experimental tests for an evolutionary trade-off between growth rate and yield in *E. coli*. *Am. Nat.* **168**, 242–251 (2006).

50. J. Orivel, P.-J. Malé, J. Lauth, O. Roux, F. Petitclerc, A. Dejean, C. Leroy, Trade-offs in an ant-plant-fungus mutualism. *Proc. Biol. Sci.* **284** (2017), doi:10.1098/rspb.2016.1679.

51. B. Dunn, T. Paulish, A. Stanbery, J. Piotrowski, G. Koniges, E. Kroll, E. J. Louis, G. Liti, G. Sherlock, F. Rosenzweig, Recurrent rearrangement during adaptive evolution in an interspecific yeast hybrid suggests a model for rapid introgression. *PLoS Genet.* **9**, e1003366 (2013).

52. M. R. Gartenberg, J. S. Smith, The nuts and bolts of transcriptionally silent chromatin in *Saccharomyces cerevisiae*. *Genetics*. **203**, 1563–1599 (2016).

53. E. R. Jerison, A. N. Nguyen Ba, M. M. Desai, S. Kryazhimskiy, Chance and necessity in the pleiotropic consequences of adaptation for budding yeast. *Nat Ecol Evol*. **4**, 601–611 (2020).

54. G. Barabás, R. D'Andrea, S. M. Stump, Chesson's coexistence theory. *Ecol. Monogr.* **88**, 277–303 (2018).

55. P. Chesson, Updates on mechanisms of maintenance of species diversity. *J. Ecol.* **106**, 1773–1794 (2018).

56. G. I. Lang, D. P. Rice, M. J. Hickman, E. Sodergren, G. M. Weinstock, D. Botstein, M. M. Desai, Pervasive genetic hitchhiking and clonal interference in forty evolving yeast populations. *Nature*. **500**, 571–574 (2013).

57. Y. Li, S. Venkataram, A. Agarwala, B. Dunn, D. A. Petrov, G. Sherlock, D. S. Fisher, Hidden Complexity of Yeast Adaptation under Simple Evolutionary Conditions. *Curr. Biol.* **28**, 515–525.e6 (2018).

58. J. Bergelson, M. Kreitman, D. A. Petrov, A. Sanchez, M. Tikhonov, Functional biology in its natural context: A search for emergent simplicity. *Elife*. **10** (2021), doi:10.7554/eLife.67646.

59. Kao KC, Sherlock G. Molecular characterization of clonal interference during adap tive evolution in asexual populations of Saccharomyces cerevisiae. Nature genetics. 2008;40(12):1499–1504.

60. Blundell JR, Schwartz K, Francois D, Fisher DS, Sherlock G, Levy SF. The dynamics of adaptive genetic diversity during the early stages of clonal evolution. Nature ecology & evolution. 2019;3(2):293–301.

61. Collins S, Bell G. Phenotypic consequences of 1,000 generations of selection at elevated CO_2 in a green alga. Nature. 2004;431(7008):566–569.

62. Perrineau MM, Gross J, Zelzion E, Price DC, Levitan O, Boyd J and Bhattacharya D. Using natural selection to explore the adaptive potential of Chlamydomonas reinhardtii. PLoS One. 2014;9(3):e92533.

63. Lee CK, Araki N, Sowersby DS, Lewis LK. Factors affecting chemical-based purification of DNA from Saccharomyces cerevisiae. Yeast. 2012;29(2):73–80.

64. Newman SM, Boynton JE, Gillham NW, Randolph-Anderson BL, Johnson AM, Harris EH. Transformation of chloroplast ribosomal RNA genes in Chlamydomonas: molecular and genetic characterization of integration events. Genetics. 1990;126(4):875–888.

65. Baym M, Kryazhimskiy S, Lieberman TD, Chung H, Desai MM, Kishony R. Inexpensive multiplexed library preparation for megabase-sized genomes. PLoS One. 2015;10(5):e0128036.

66. Ghodsi M, Liu B, Pop M. DNACLUST: accurate and efficient clustering of phylogenetic marker genes. BMC Bioinformatics. 2011;12:271.

67. Li H, Durbin R. Fast and accurate short read alignment with Burrows-Wheeler transform. Bioinformatics. 2009;25(14):1754–1760.

68. Ba ANN, Cvijović I, Echenique JIR, Lawrence KR, Rego-Costa A, Liu X, Levy SF and Desai MM. High-resolution lineage tracking reveals travelling wave of adaptation in laboratory yeast. Nature. 2019;575(7783):494–499.

69. Zhu YO, Siegal ML, Hall DW, Petrov DA. Precise estimates of mutation rate and spectrum in yeast. Proc Natl Acad Sci U S A. 2014;111(22):E2310–8.

70. Barillot E, Lacroix B, Cohen D. Theoretical analysis of library screening using a N-dimensional pooling strategy. Nucleic Acids Res. 1991;19(22):6241–6247.

71. Baym M, Shaket L, Anzai IA, Adesina O, Barstow B. Rapid construction of a whole-genome transposon insertion collection for Shewanella oneidensis by Knockout Sudoku. Nature communications. 2016;7(1):1–13.

72. Manhart M, Adkar BV, Shakhnovich EI. Trade-offs between microbial growth phases lead to frequency-dependent and non-transitive selection. Proc Biol Sci. 2018;285(1872).

73. Desai MM, Fisher DS. Beneficial mutation-selection balance and the effect of linkage on positive selection. Genetics. 2007;176(3):1759–1798.

74. Pawitan Y. In All Likelihood: Statistical Modelling and Inference Using Likelihood. Oxford science publications. OUP Oxford; 2001.

75. Hunter GA, Ferreira GC. Molecular enzymology of 5-aminolevulinate synthase, the gatekeeper of heme biosynthesis. Biochim Biophys Acta. 2011;1814(11):1467–1473.

76. Brown BL, Kardon JR, Sauer RT, Baker TA. Structure of the Mitochondrial Aminolevulinic Acid Synthase, a Key Heme Biosynthetic Enzyme. Structure. 2018;26(4):580–589.e4.

77. Betts MJ, Russell RB. Amino-acid properties and consequences of substitutions. In: Bioinformatics for Geneticists. Chichester, UK: John Wiley & Sons, Ltd; 2007. p. 311–342.

Acknowledgements

We thank Gavin Sherlock and Katja Schwartz for providing the barcoded yeast library, Stephen Mayfield and Frank Fields for laboratory equipment and help with algal husbandry, Rachel Dutton and Manon Morin for help with sequencing, Scott Rifkin and Jessica Bloom for help with microscopy, Justin Meyer, Alena Martsul, Shohreh Sikaroodi for technical assistance, the Kryazhimskiy, Meyer and Hwa labs, Damien Barret, Josh Borin, Shermin de Silva, Susanne Dunker, Nandita Garud, Stan Harpole, Canan Karakoç, Holly Moeller, Dmitri Petrov, and Peter Zee for feedback. Sequencing was done in part at the UCSD IGM center (University of California, San Diego, La Jolla, CA). We acknowledge the San Diego Supercomputing Center for the use of the TSCC cluster for computing services.

Funding:

National Science Foundation CAREER grant 1846376 (EFYH)

Deutsches Zentrum für Integrative Biodiversitätsforschung (iDiv) grant DFG–FZT 118, 202548816 (EFYH)

BWF Career Award at the Scientific Interface grant 1010719.01 (SK)

Alfred P. Sloan Foundation grant FG-2017-9227 (SK)

Hellman Foundation (SK)

Author contributions:

Conceptualization: SV, EFYH, SK

Methodology: SV, HYK, SK

Investigation: SV, HYK, SK

Visualization: SV, HYK, SK

Funding acquisition: EFYH, SK

Project administration: SK

Supervision: EFYH, SK

Writing - original draft: SV, SK

Writing - review and editing: SV, HYK, EFYH, SK

Competing interests: The authors declare no competing interests.

Data and materials availability.

All raw sequencing data is available on the US National Center for Biotechnology Information (NCBI) Sequence Read Archive (SRA) under BioProject PRJNA735257. Other input data (e.g. growth data, variant calls, community yield etc) and analysis scripts can be found in Data Files S1–S3 and on Dryad at https://doi.org/10.6076/D14K5X .The latest version of the barcode counting software BarcodeCounter2 can be found at https://github.com/sandeepvenkataram/BarcodeCounter2.git

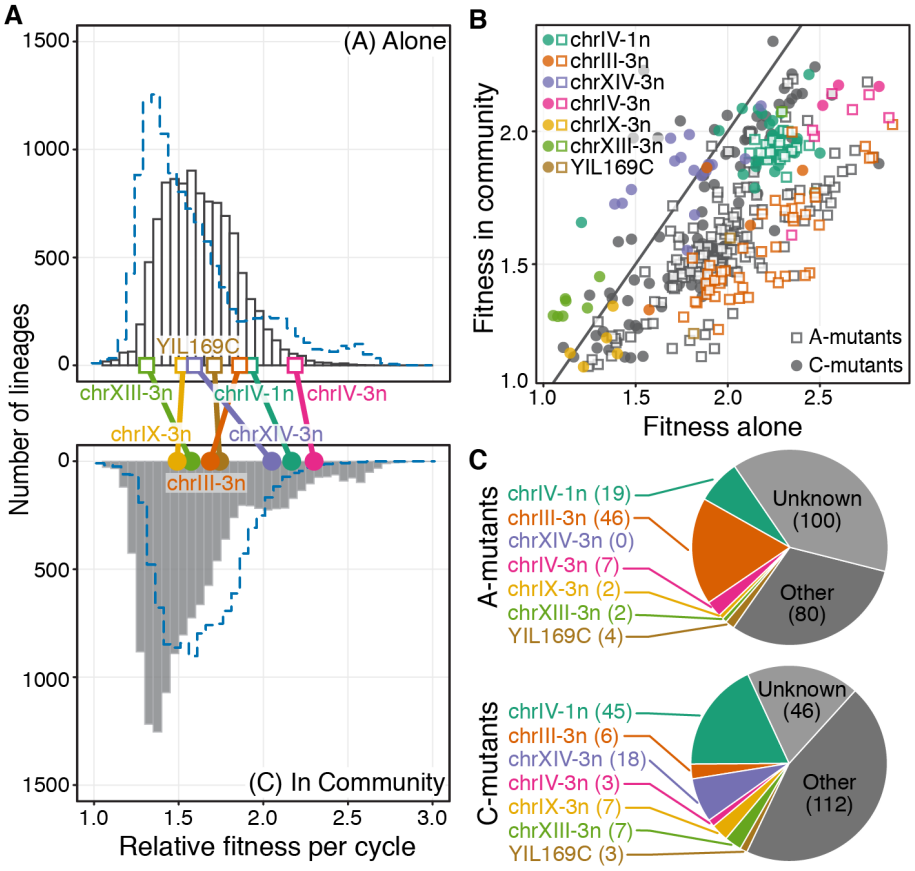

Figures

Figure 1. Ecological interactions with alga alter adaptation in yeast at fitness and genetic levels. (A) Yeast bDFE when evolving alone (top) and in the community with alga (bottom). Each histogram is constructed based on five replicates of the BLT experiment. Dashed blue lines show the outlines of the bDFE in the other condition. Each colored point indicates the average fitness of a mutant carrying a mutation at the indicated adaptive locus (same data as in panel B, see *SM* for details). Large copy-number variants are referred to as chr*x*-*y*n, where *x* is the chromosome number and *y* is the number of copies. **(B)** Fitness of A- and C-mutants measured in competition assays in the A- and C-conditions. Mutants carrying mutations at the 7 most common driver loci are colored. **(C)** Distribution of adaptive mutations among A- and C-mutants. The same 7 most common mutation classes are shown explicitly as in panels A and B, all other classes are grouped into "Other" (see Data S3 for full distributions). Adaptive mutations that are expected to be present in our mutants but are not identified are labelled as "Unknown" (see *SM* for details). The number of times each locus was independently mutated is given in parentheses.

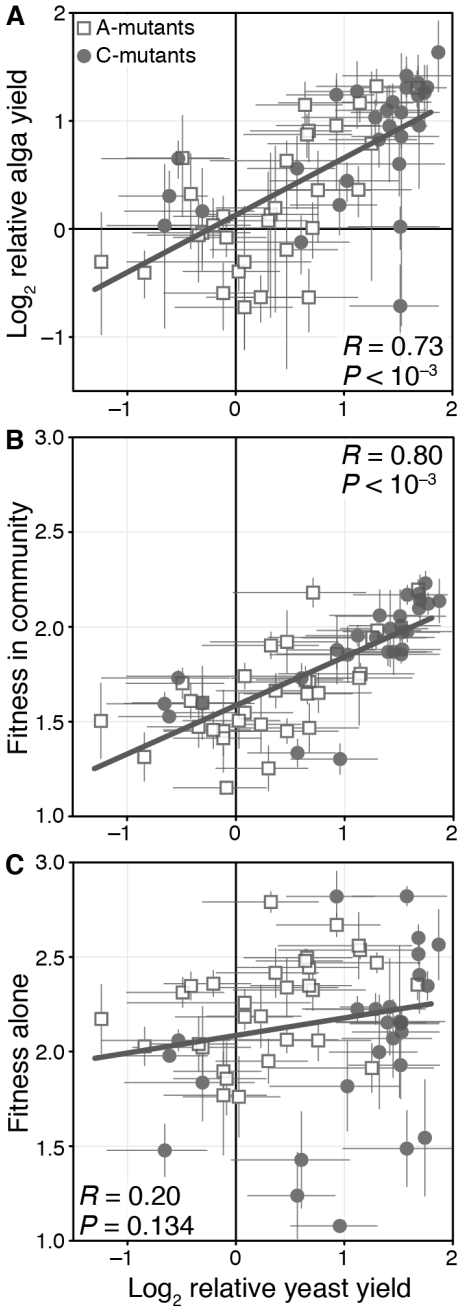

Figure 2. Relationship between yields and fitness. (A) Correlation between yeast and alga yields across communities formed by mutant yeast and ancestor alga ("mutant communities"). **(B)** Correlation between mutant fitness in the original community (C-condition) and yeast yield in mutant communities. **(C)** Correlation between mutant fitness alone (A-condition) and yeast yield in mutant communities.

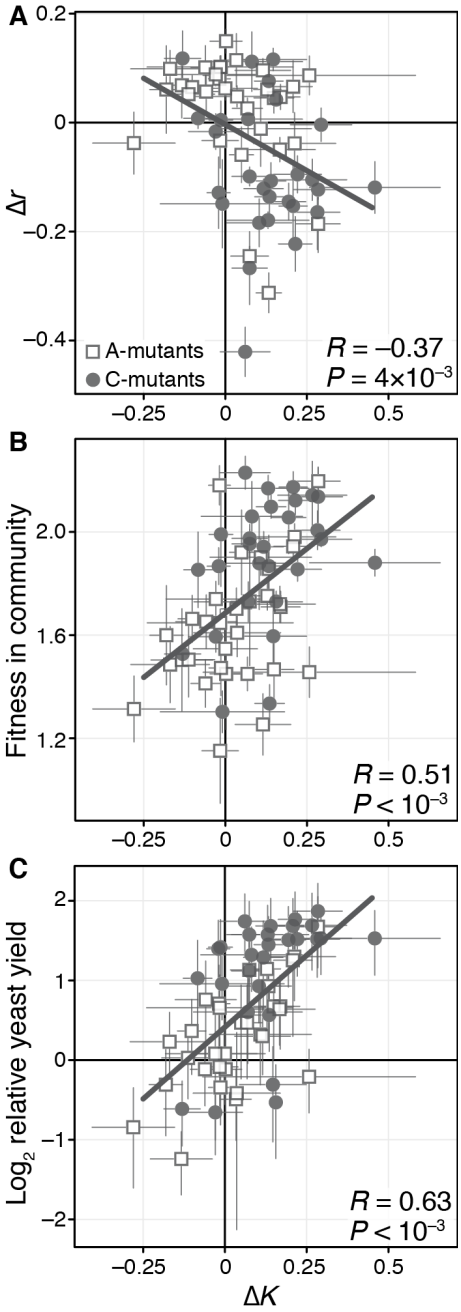

Figure 3. Relationships between the effects of adaptive mutations on growth parameters, fitness and yield. The mutational effects Δr and ΔK are reported as fractional differences relative to the ancestral values (see *SM*). **(A)** Correlation between ΔK and Δr among adapted mutants. (**B)** Correlation between ΔK and their relative fitness in the original community among adapted mutants. (**C)** Correlation between ΔK and yeast yield in mutant communities.

Supplementary Materials

Supplementary Text

References 55 to 72

Figure S1. Growth curves for the ancestral strains of the yeast and the alga.

Figure S2. Lineage trajectories in yeast populations in the A-condition.

Figure S3. Lineage trajectories in yeast populations in the C-condition.

Figures S4. Estimation of fitness of adapted lineages in the BLT data.

Figure S5. Evidence for pre-existing mutations in the BLT experiments.

Figures S6. Lineage frequency trajectories in the competition assay.

Figures S7. Correlation between fitness estimates across replicates of the competition assay.

Figures S8. Mean and coefficient of variation of the fitness estimates in the competition assay.

Figures S9. Correlation between BLT and competitive fitness estimates.

Figures S10. An example illustrating the detection of large chromosomal duplications and deletions in the genome sequence data.

Figures S11. Relationship between coverage and chromosome position.

Figures S12. Allele frequency spectrum for ancestral and adapted isolates.

Figures S13. Distribution of mutations per clone.

Figures S14. Distribution of adaptive mutations across the most common driver loci.

Figures S15. The log-likelihood function for the estimation of the chrIII-3n beneficial mutation rate.

Figures S16. Sampling probabilities for adaptive mutations at the most common driver loci.

Figures S17. Correlation between yield measurements across replicates.

Figures S18. Correlation between yeast mutant fitness in the original community and alga yield in the mutant community.

Figures S19. Estimated yeast and alga yields among random A- and C-mutants.

Figures S20. Representative microscopy image showing lack of physical associations between yeast and alga cells.

Figures S21. Mutant growth curves in the A-condition.

Figures S22. Correlation between replicates for *r* and *K* measurements.

Figures S23. Relationship between growth parameters, yields and fitness.

Table S1. Statistics of mutational counts among sequenced mutants.

Table S2. Number of isolates carrying the most common adaptive mutations and the estimated mutation rates.

539

540 **Data S1.** List of all sampled isolates, their fitness, phenotypes and yields.

541 **Data S2.** List of all identified mutations.

542 **Data S3.** Distribution of adaptive mutations across driver loci.

Supplementary Material for "Early adaptation in a microbial community is dominated by mutualism-enhancing mutations"

Sandeep Venkataram, Huan-Yu Kuo, Erik F. Y. Hom, Sergey Kryazhimskiy*

July 7, 2021

Contents

1 Data availability **3**

2 Barcode lineage tracking (BLT) experiment and data analysis **3**
2.1 Strains . . . 3
2.2 Growth conditions . . . 3
2.3 BLT experiment . . . 4
2.4 Justification for ignoring adaptation in alga . . . 5
2.5 Barcode sequencing . . . 5
2.6 BLT data analysis . . . 7
2.7 Results . . . 11

3 Competitive fitness assays **11**
3.1 Clone isolation and barcode genotyping . . . 11
3.2 Competition assay experiment . . . 12
3.3 Competition assay data analysis . . . 13
3.4 Results . . . 13

4 Genome sequencing and analysis **15**
4.1 DNA extraction and library preparation and sequencing . . . 15
4.2 Identification of new mutations . . . 15
4.3 Identification of driver loci carrying small adaptive mutations . . . 17
4.4 Probability of genetic parallelism . . . 18
4.5 Results . . . 18

*Correspondence: skryazhi@ucsd.edu

5 Simulations of evolutionary dynamics and the estimation of rates of adaptive mutations **20**
5.1 Data 21
5.2 Model 22
5.3 Results 24

6 Phenotyping **25**
6.1 Measurements of species yields in mutant communities 25
6.2 Microscopy 26
6.3 Mutant growth curve measurements 26
6.4 Statistical analysis 27

7 Possible function effects of mutations in *HEM1*, *HEM2* and *HEM3* genes **28**
7.1 HEM1 28
7.2 HEM2 30
7.3 HEM3 31

8 Supplementary Figures **32**

9 Supplementary Tables **55**

1 Data availability

All raw sequencing data is available on the US National Center for Biotechnology Information (NCBI) Sequence Read Archive (SRA) under BioProject PRJNA735257. Other input data (e.g. growth data, variant calls, community yield etc) and analysis scripts can be found on Dryad at

https://doi.org/10.6076/D14K5X.

The latest version of the barcode counting software BarcodeCounter2 can be found at

https://github.com/sandeepvenkataram/BarcodeCounter2.git.

2 Barcode lineage tracking (BLT) experiment and data analysis

2.1 Strains

We used the strain CC1690 of the alga *Chlamydomonas reinhardtii* as in Ref. [32], which can also be obtained from the Chlamydomonas Resource Center.

The barcoded library of the diploid yeast *Saccharomyces cerevisiae* strain GSY6699 is described in Ref. [37] and was kindly provided by Prof. Gavin Sherlock. This is a diploid, prototrophic strain derived from the BY genetic background, homozygous throughout the genome, except for locus YBR209W, where one copy of a DNA barcode was integrated, as described in Ref. [35]. Our starting library consists of about 5×10^5 clones, each of which carries a unique DNA barcode at this locus. In principle, the genomes of all clones should be identical everywhere else prior to our barcode lineage tracking (BLT) experiment. However, as discussed in detail below (see Sections 2.6.2 and 4), we found that our initial population already contains some pre-existing polymorphisms, which arose prior to our BLT experiment.

2.2 Growth conditions

Both yeast monocultures and yeast-alga communities were cultured in a defined basic medium ("CYM medium", see Ref. [32]) supplemented with 2% dextrose, 10mM KNO_2 and 0.5mM NH_4Cl, which we thereafter refer to as the "growth medium". All cultures were grown at room temperature (21°C) on a platform shaker with 70 foot-candles of constant light (three Feit Electric #73985 suspended approximately 24 inches above the platform shaker) shaking at 125 RPM, unless noted otherwise.

When yeast is grown alone in this medium (the A-condition), it reaches the final density of 2.49×10^6 cells per mL. When yeast and alga are co-cultured together (the C-condition), yeast and alga reach final densities (yields) of 2.72×10^6 cells per mL and 5.63×10^5 cells per mL, respectively. In all subsequent experiments, we grow our cultures in 10mL of the growth medium in 50mL flasks, unless otherwise noted.

2.3 BLT experiment

2.3.1 Pre-cultures

Prior to the BLT experiment, yeast and alga were pre-cultured in 50mL of growth medium in 250mL delong baffled flasks (PYREX #C4446250) for two and 10 days respectively. Alga pre-cultures were started from colonies. To start yeast pre-cultures, the barcoded yeast library was thawed from frozen stock at room temperature, then 500µL were transferred into 50mL of the growth medium.

2.3.2 Initiation and propagation

We conducted five replicate BLT experiments for each of two treatments, yeast monoculture (the A-condition) and yeast + algae community (the C-condition). All BLT experiments were conducted in 10mL of the growth medium in 50mL Erlenmeyer flasks (FisherSci #FS2650050) capped with 50mL plastic beakers (VWR #414004-145) to maintain sterility. Each monoculture BLT experiment was initiated from 100µL of the yeast pre-culture. Each community BLT experiment was initiated from 100µL of the 1:1 (v/v) yeast and alga mixture. During the BLT experiment, cultures were grown on a platform shaker with constant light as described above for 5 days before being diluted 1:100 for the next growth cycle (100µL into 10mL fresh media). A total of 17 growth/dilution cycles were completed.

2.3.3 Culture preservation

Glycerol stocks were taken of the yeast pre-culture and yeast + algae inoculum mixture, as well as at the end of every odd growth cycle. Separate stocks were stored for DNA extraction and cell isolation purposes with two replicates each, for a total of 4 stocks per culture per time point. Cell isolation stocks were created by aliquoting 1.5mL of culture into 500µL of 80% glycerol, mixing by vortex and storing at −80°C. DNA stocks were created by removing the supernatant of the remaining 7mL of culture via centrifugation and resuspending in 2mL of 20% glycerol (80% glycerol diluted with 1x PBS), which was then stored as two separate 1mL stocks at −80°C.

2.4 Justification for ignoring adaptation in alga

Here we argue that ignoring adaptation in alga in our experiment is justified, based on our current knowledge of rates of adaptation in yeast and alga.

In the C-condition, that is, when yeast and alga are co-cultured together, yeast and alga reach final yields of 2.72×10^7 and 5.63×10^6 cells, respectively, with the bottleneck sizes being by a factor of 100 smaller. Since there is no evidence of alga or yeast death in this condition (Figure S1), we estimate that both species undergo on average $\log_2 100 = 6.64$ doublings per cycle. Numerous evolution experiments with yeast populations of comparable or smaller size across various environmental conditions have shown that adaptive mutations arise and reach high frequencies within 250 generations or less [26, 35, 56, 59, 60]. Although much less is known about the rates of adaptation in *Chlamydomonas reinhardtii*, one study reports a failure of the alga (strain CC2344) to adapt within 1000 generations of evolution at the bottleneck size of 10^5 cells, i.e., twice as large as in our experiment [61]. Another study reports 35% growth rate gain after 1880 generations of evolution in alga strain CC-503 cw92 mt+ [62], although the bottleneck size in that experiment was about 20 times larger than in ours and detectable gains appeared only after about 300 generations. These studies suggest that yeast has a much larger potential to gain adaptive mutations than alga, at least in laboratory conditions.

2.5 Barcode sequencing

2.5.1 DNA isolation

DNA stocks were thawed and DNA isolated using a "salting out" method, based on methods from Refs. [63, 64]. The thawed stocks were first centrifuged, and the supernatant removed. The pellet was resuspended in 300µL 3% SET buffer (3% SDS, 10mM EDTA, 30mM Tris) and incubated at 65°C for 15 minutes. The tube was cooled to room temperature by immersing in room temperature water, then 2.5µg of RNAse A was added. After vortexing, the mixture was incubated at 37°C for 1 hour, after which it was cooled on ice. 150µL of 3M Sodium Acetate was then added and mixed by inversion, after which it was cooled on ice for a further 5 minutes before centrifuging at maximum speed for 10 minutes on a tabletop centrifuge. The supernatant was transferred to a new tube and DNA was precipitated by the addition of 500µL isopropanol, which was mixed by inversion and then pelleted by centrifugation for 1 minute at maximum speed. The supernatant was removed and the pellet was washed with 200µL cold 70% ethanol without vortexing before being allowed to dry inverted for 30 minutes at room temperature before the DNA was resuspended in 50µL molecular biology grade water.

2.5.2 Sequencing library preparation

The barcode locus was amplified through a 2-step PCR protocol, slightly modified from the protocol described in Ref. [36]. The first amplification added inline indices for sample multiplexing, universal molecular identifiers for removing PCR duplicates during analysis and Illumina-compatible adapter sequences for a second round of amplification with standard Illumina Nextera XT primers. For the first reaction, 10µL of template was mixed with 25µL of OneTaq 2x Master Mix, 1µL of 25mM $MgCl_2$, 1µL each of the forward and reverse primers (at 10mM concentration) and 12µL of molecular biology grade water. Primer sequences are as described in Ref. [36]. This mixture was amplified using the following conditions:

1. 94°C for 10 min
2. 94°C for 3 min
3. 55°C for 1 min
4. 68°C for 1 min
5. Repeat steps 2–4 for a total of 8 cycles
6. 68°C for 1 min
7. Hold at 4°C

The amplified product was purified using Ampure XP magnetic beads following the protocol in Ref. [65] (with 50µL of beads used per sample). Then, 10µL of the purified product was used as the template for a second reaction along with Illumina Nextera XT primers (1µL of 10mM stock for each primer), 1µL of 25mM $MgCl_2$, 25µL of OneTaq 2x Master Mix and 12µL of water with the following reaction conditions:

1. 94°C for 5 min
2. 94°C for 30 sec
3. 62°C for 30 sec
4. 68°C for 30 sec
5. Repeat steps 2–4 for a total of 25 cycles
6. 68°C for 5 min
7. Hold at 4°C

The PCR products were purified using Ampure XP beads as before. 5µL of each sample was mixed to form a pool for Illumina sequencing, concentrated using Ampure beads as before with equal volume of beads as pooled sample, size selected via agarose gel extraction to isolate the correct amplicon before submitting for sequencing.

2.5.3 Sequencing

Populations 1 and 6 were initially sequenced on a MiSeq platform. All populations (including 1 and 6) were then also sequenced on a HiSeq platform. Data from both runs were combined for all downstream analysis of frequency trajectories. We obtained an average of 2.6 million paired-end reads per time point.

2.6 BLT data analysis

2.6.1 Barcode identification and counting

To identify and count DNA barcodes, we used a custom python pipeline BarcodeCounter2 available at https://github.com/sandeepvenkataram/BarcodeCounter2. The package first uses the BLASTn tool to identify sequences known to flank the barcode region within each read pair. If reads contain inline indices, samples can be demultiplexed. Universal molecular identifier (UMI) sequences can be extracted if present within the reads. If a sequence contains multiple barcode regions, these extracted regions are concatenated together. To account for sequencing errors, DNAClust [66] is then used to cluster the concatenated barcodes into clusters of nearly identical sequences which presumably originated from the same DNA molecule. The output of DNAClust is a FASTA database of all unique barcode sequences present in the library. Then, BWA [67] is used to map the barcode sequences from each sample onto the clustered FASTA database. Mapping of reads is necessary because the clustering process removes identifying information associating barcode sequences with samples from which they came. PCR duplicates are removed based on the UMI sequences, and the total number of unique reads corresponding to every barcode in the FASTA database is counted. The final output is a tab-delimited table of the read counts for every barcode in every sample. The software is designed to be user-friendly and highly customizable, with simple text files describing the input files, multiplexed samples and a sequence template describing the structure of the sequenced reads. The package is built using python3, and uses the popular BioPython package. The package has multithreading support, and can be run on both personal computers and supercomputing clusters.

When generating the database of all unique barcode sequences, we clustered sequences at 95% similarity, so that, given that the length of our barcode is 52bp, sequences with 3 or more basepair differences were merged into the same cluster. This set of clustered sequences was generated only once using all of the time points from all sequenced populations. Using this method, we identified a total of 557,087 unique barcodes in our data

with about 527,745 barcodes present at the initial time point, consistent with [35]. The number of detected barcodes gradually declines over time, as would be expected in the presence of demographic stochasticity and adaptive evolution (Figures S2B and S3B). Since only roughly 68,475 are detectable in any population by cycle 11 (i.e., about 13% of those present initially), we constrained our subsequent analysis to cycles 1 through 11.

2.6.2 Identification of adapted lineages and estimation of their fitness

The raw barcode frequency data for all our populations are shown in Figures S2, S3 (note that populations were sequenced only at odd cycles 1, 3, 5, 7, 9, 11, 13, 15 and 17). Our goal in analyzing these data was two fold. First, in order to physically isolate yeast clones that carry adaptive mutations (see Section 4), we needed to identify those yeast lineages that acquired an adaptive mutation (adapted lineages) among those that did not (neutral lineages). Second, in order to construct the distributions of fitness effects of beneficial mutations (bDFEs), we needed to estimate the competitive fitness of adapted lineages relative to the ancestoral yeast strain.

We were unable to successfully apply the BLT data analysis methods developed previously [35, 68] to our data primarily because of the high extinction rate of our barcodes. Thus, we developed a new iterative heuristic procedure described below that overcomes this problem. Direct fitness measurements of isolated clones (see Section 3) confirmed that the heuristic procedure works well.

Iterative heuristic procedure for identification of adapted lineages and estimating their selection coefficients.

1. **Initialization.** Neutral barcodes for iteration 1 are identified separately for every pair of consecutive time points. For a given time point pair, we define the set of neutral lineages at iteration 1 as those lineages whose frequency (a) does not exceed 10^{-4} at the earlier time point and (b) increases by less than 100-fold between cycle 1 and cycle 11.

2. **Estimation of mean fitness.** Given the set of neutral lineages at iteration $k-1$, we obtain their total frequency $x_{\text{neut}}^{(k-1)}(t)$ at each cycle t. The frequency of neutral lineages is governed by equation

$$x_{\text{neut}}(t+1) \approx x_{\text{neut}}(t)e^{-\bar{s}(t)},$$

where $\bar{s}(t)$ is the mean selection coefficient (per cycle) of the population at cycle t. Thus, we estimate the mean selection coefficient of the population at cycle t at iteration k as

$$\bar{s}^{(k)} = -\log \frac{x_{\text{neut}}^{(k-1)}(t+1)}{x_{\text{neut}}^{(k-1)}(t)}.$$

The mean fitness at cycle t is then defined as $1 + \bar{s}^{(k)}(t)$.

3. **Estimation of fitness of individual lineages.** The frequency $x_i(t)$ of lineage i with selection coefficient s_i (per cycle) relative to the ancestor is governed by the equation

$$x_i(t+1) = x_i(t)\, e^{s_i - \bar{s}(t)} = x_i(t)\, \frac{x_{\text{neut}}(t+1)}{x_{\text{neut}}(t)}\, e^{s_i}.$$

Thus, for every lineage i (including those that were called as neutral at the previous iteration) we estimate $s_i^{(k)}$ at iteration k at time point t as

$$s_i^{(k)}(t) = \log \frac{x_i(t+1)}{x_{\text{neut}}^{(k-1)}(t+1)} - \log \frac{x_i(t)}{x_{\text{neut}}^{(k-1)}(t)}. \tag{1}$$

These estimates are made for every pair of consecutive time points between cycles 1 and 11. If $x_i(t) = 0$ and $x_i(t+1) = 0$, the time point pair is excluded from the calculations. If only one of the two frequencies is 0, then this frequency is set to 0.5 / total read depth. To obtain the final estimate of the selection coefficient $s_i^{(k)}$ for lineage i at iteration k, we average all $s_i^{(k)}(t)$, weighting each $s_i^{(k)}(t)$ by the number of reads for lineage i at time t. We calculate the standard error $\sigma_i^{(k)}$ with the same weighting. The relative fitness of lineage i is then defined as $1 + s_i^{(k)}$.

4. **Calling adapted lineages.** Lineage i is called adapted at iteration k if $s_i^{(k)} > 2\sigma_i^{(k)}$.

5. **Updating the set of neutral lineages.** We calculate the coefficient of variation for each lineage i as $\text{CV} = \sigma_i^{(k)}/s_i^{(k)}$. We include any lineage i into the new set of neutral lineages at iteration k if (a) its maximum frequency does not exceed 10^{-4} between cycles 1 and 11, and (b) either the CV of the lineage is more the median CV across all lineages or if $s_i^{(k)} < 0$ (see Figure S4A).

6. **Termination.** The procedure is terminated when the set of neutral lineages at iteration k differs by less than 5% compared to the set at the iteration $k-1$.

Our procedure converges to a stable set of neutral lineages within 5 iterations. We report fitness values relative to the ancestral strain on a per-cycle basis, rather than the per-generation basis typically used in the literature because our cultures experience growth phases other than exponential growth, as discussed in Refs. [36, 57].

Validation. We performed two "sanity" checks to ensure that our analysis gives reasonable results. First, mean fitness is expected to monotonically increase over time in each population. We find that mean fitness does indeed increase monotonically during the first 11 cycles in all but one populations (Figure S4B). Second, we visually inspected how well individual lineage trajectories are fitted by equation (1) and found that these fits are generally very good (Figure S4C,D shows typical fits).

Pre-existing mutations. Some mutations could have arisen prior to the beginning of the experiment, specifically, prior to splitting the barcoded yeast library between five A and five C replicates. Such pre-existing mutations cause two issues with the downstream analysis and interpretation. First, they make it more difficult to identify causal mutations that increase fitness of adapted lineages. We discuss this problem and how we address it in Section 4. The second issue is that pre-existing beneficial mutations confound the inference of bDFEs and their comparison across treatments. Specifically, if multiple lineages (within the same population or in different replicate populations) carry the same pre-exisiting beneficial mutation and are identified as such, this mutation will be counted multiple times and will therefore inflate the size of a fitness class in the inferred bDFE.

To diagnose this problem, we note that there are two types of pre-existing mutations. Those that arose after the transformation that introduced barcodes into our strain (type I) and those that arose before this transformation (type II). All pre-existing mutations of type I are linked to different barcodes. Therefore, these mutations can be identified by comparing barcodes of lineages identified as adapted in different populations. We found that pairs of populations have on average 416 (15%) adapted lineages with a common barcode, whereas only 23 (0.8%) would be expected by chance (Figure S5). Barcodes are more often shared between A populations than other types of population pairs (22% vs 13%, t-test $P = 10^{-10}$). We suspect that this is because the majority of adapted mutants have higher relative fitness in the A-condition than the C-condition (Figure 1B in the main text), such that pre-existing mutations are more likely to reach high frequencies and be detected in the A-condition. We eliminate pre-existing beneficial mutations of type I from our bDFE analysis by constructing these distributions from lineages with unique barcodes.

The same pre-existing mutation of type II can be linked to multiple barcodes and is indistinguishable in the barcode data from multiple independently arising mutations. However, pre-existing mutations of type II can be identified in the genome sequencing data. As discussed in Section 4.5, we find no evidence of such mutations, suggesting that they must be rare in our populations.

2.6.3 Permutation tests for differences in bDFE across conditions

We randomly relabel adaptive lineages as being from either the A- or C-condition, and calculate the difference in bDFE median and IQR from this permuted data. This procedure was conducted 10,000 times, to generate a random distribution of median and IQR difference values. The observed median and IQR difference were larger than those of all permuted values.

2.7 Results

The median standard error in our estimates of fitness of adaptive mutants was 0.02, and median CV was 0.08 (Figure S4A). The standard deviation of the bDFEs is much larger, 0.22 for A populations and 0.33 for C populations, suggesting that there are multiple classes of adaptive mutations available to yeast in both conditions.

3 Competitive fitness assays

3.1 Clone isolation and barcode genotyping

We selected cycle 9 to isolate adapted mutants because the estimated fraction of adapted lineages in our evolving populations was large, but each adapted lineage was still at a low frequency (Figures S2 and S3). Specifically, 92% of a typical population in the A-condition consisted of adapted lineages, with the median frequency of an individual adapted lineage being 9×10^{-5} ($\sim$ 22 cells per lineage at the bottleneck), and 73% of a typical population in the C-condition consisted of adapted lineages, with the median frequency of an individual adapted lineage being 7×10^{-5} ($\sim$ 19 cells per lineage at the bottleneck).

Isolation of random clones. To isolate adapted clones, frozen stocks of the monoculture and community populations from cycle 9 were thawed, plated onto standard 100mm Petri dishes with CYM + 1% agarose at a dilution of approximately 100 cells per dish, and incubated at 30°C for three days (algae do not grow at 30°C). 88 random colonies were isolated from each population, i.e., a total of 440 clones from the A- and C-condition each. Eight additional clones from each population were harvested at cycle 17 and are present in the pools described below, but they are not included in any of the analyses presented in this study. Each colony was transferred into a well of a 96-well plate (Corning 3370) with 200µL of CYM media and incubated for two days at 30°C. 10µLwas used for each of the "population", "row" and "column" pools described below. Then, 50µL of 80% glycerol was added to each well, and the plate was stored at −70°C.

Barcode genotyping. The DNA barcodes of all isolated clones were identified by sequencing, using the Sudoku method [70, 71]. Specifically, 10µL of each clone was pooled into 10 "population" pools (one pool for each source population), eight "row" pools and 12 "column" pools. DNA barcodes in each pool were amplified and sequenced as described in Section 2.5. We expect that a given combination of row, column and population pools would have a single barcode in common, defining the isolate in the corresponding well of the appropriate plate. We determined all barcodes present in the intersection of each combinations of row, column population pool. If a single barcode is identified in the intersection, the corresponding well is assigned that barcode identity. If multiple barcodes or no barcode are identified, the associated clone is removed from further analysis.

Generation of A, C and N pools. We used the heuristic procedure described in Section 2.6.2 to classify clones with identified barcodes into three groups described below: non-adapted, adapted in the C-condition or adapted in the A-condition. Clones were pooled into three libraries defined by their membership in these three groups as follows. To construct each pool, we transferred 20µL of thawed frozen stock of each isolate into a 2mL 96-deep-well plate (Corning P-2ML-SQ-C) filled with 1.8mL of growth media supplemented to 10mM ammonia. After incubating these plates at 30°C for three days, we formed each pool by combining 200µL of individual saturated cultures. Three pools were stored in 20% glycerol at −70°C.

For the sake of efficiency, clone pooling was based on an earlier version of the heuristic procedure described in Section 2.6.2 used for the classification of lineages. The current version of the procedure (as described in Section 2.6.2) classifies lineages slightly differently. As a result, pools do not perfectly correspond to the classification of clones according to the current heuristic procedure, which is provided below. This minor discrepancy has no bearing on our results because the final classification of clones is based on fitness estimates from the competition assays (see Section 3.3). The *A pool* contains 214 clones that are classified as adapted in A populations. The *C pool* contains 223 clones that are classified as adapted in C populations. The *N pool* contains 144 clones, 84 of which are classified as neutral from the BLT analysis (i.e., not adapted in either A or C populations), 29 clones that are classified as adapted in the A-condition and 31 clones that are classified as adapted in the C-condition. Thus, we measured competitive fitness for a total of 581 clones.

3.2 Competition assay experiment

To conduct the competitive fitness assays, we pre-cultured each of the three pools (N, A and C; see above) separately in the growth media for two days. We also pre-cultured algae for 10 days, starting from colonies. We then combined A, C and N pools in the 1:1:18 ratio. We carried out three replicate competitions in the A-condition and three replicate competitions in the C-condition. To this end, we inoculated each of the six replicates with 100µL of the combined A/C/N pool. In addition, the three C-condition replicates were inoculated with 100µL of the algae preculture ($\sim 10^6$ cells / mL).

All replicates were propagated in conditions identical to the BLT experiment for a total of five growth cycles. Glycerol stocks were made at the end of each growth cycle after the dilution step by centrifuging the full culture volume, removing the spent media and resuspending the pellet in 2mL of 20% glycerol + PBS. Two 1mL aliquots of this glycerol suspension were stored at −70°C. One of these aliquots was harvested for DNA extraction and barcode sequencing using protocols described in Section 2.6.2.

3.3 Competition assay data analysis

Barcodes were identified and counted as described above (see Section 2.6.1). The resulting barcode count data were analyzed as described in Ref. [36] using software available at https://github.com/barcoding-bfa/fitness-assay-python. Briefly, the 84 non-adapted barcodes (as defined from the BLT analysis described in Section 2.6.2) from the N pool were used to estimate the mean fitness trajectories and the additive and multiplicative noise parameters for each pair of time points in each assay (see Ref. [36] for details). These estimates were used to estimate the fitness of every lineage the assay for each pair of neighboring time points along with the error in the estimate. The variance of an estimate for a given pair of time points was calculated as the inverse of the read depth at the earlier of the two timepoints + the estimated multiplicative noise parameter. Inverse variance weighting was then used to combine estimates across all time point pairs to generate a single fitness and error estimate for each lineage in each replicate. Replicate estimates were combined using further inverse variance weighting to generate the final fitness estimate for each isolate in the A- and C-conditions. For each mutant in each condition, we also calculated the 95% confidence interval around the fitness estimate based on the variability in fitness measurements between replicates (assuming that measurement errors are distributed normally).

3.4 Results

We obtained barcode frequency data at cycles 1, 2, 3, 4 and 5 (Figure S6). Fitness estimates of individual lineages were concordant between replicates (Figure S7), with relatively low estimation errors (Figure S8). Estimated fitness of sampled clones in both conditions along with errors and confidence intervals are provided in Data S1.

Determining valid clones for further analysis. Of the 581 clones that were pooled in the competition assays, we filtered out many clones from downstream analysis via a number of filters. First, clones that were sampled at cycle 17 were excluded from further analysis, as were clones that lacked a valid fitness measurement in either environment or had variance in fitness measurement in either environment ≥ 0.5. These filters removed 151 of 581 from consideration, leaving us with 430 clones for further analysis.

Calling adapted clones. We use the competition assay data to call adapted clones. A clone is called as adapted in a given environment if its estimated competitive fitness in that environment is more than two standard errors greater than 1 (2.3% FDR based on normal distribution). We identified 401 clones as adapted in the A-condition (see Data S1). 221 of them were sampled from the A-condition and we refer to them as the A-mutants. We identified 402 clones as adapted in the C-condition (see Data S1). 189 of them were sampled from the C-condition and we refer to them as the C-mutants. There

are 16 clones that are not adapted in either A or C condition, 13 clones that are adapted in the C-condition but not in the A-condition and 12 clones that are adapted in the A-condition but not in the C-condition. Of the 16 clones not adapted in either the A or C conditions, 12 come from lineages determined not to be adaptive in the BLT analysis, which we define as our neutral clones (Data S1). The genomes of 215 A-mutants, 181 C-mutants and eight neutral mutants were later sequenced, as described in Section 4.

Relationship between fitness estimated in competition assays and in BLT experiments. The correlation between fitness of adapted mutants (i.e., A- and C-mutants) estimated in the competition assays and those estimated from the BLT data is reasonably good (Figure S9, $R = 0.57$, $P = 8.77 \times 10^{-37}$), but there are also some systematic differences. Specifically, competition assays over-estimate BLT fitness in the A-condition and under-estimate it in the C-condition (Figure S9). We discuss possible reasons for these discrepancies below.

When we place mutants onto the bDFE in the non-home environment (as in Figure 1A in the main text) and when we estimate the probability of sampling a mutation in the non-home environment (see Section 5), we need to know the BLT fitness of mutants in their non-home environment. We have no direct measurements of BLT fitness of A- or C-mutants in their non-home environment, but we do have the non-home fitness estimates of all mutants in competition assays. However, directly substituting BLT fitness for competitive fitness would lead to biases due to the aforementioned discrepancies between the two estimates. To correct for these discrepancies, we linearly regress BLT fitness of A-mutants against their competitive fitness in the A-condition and we regress BLT fitness of C-mutants against their competitive fitness in the C-condition (see Figure S9). We then use these regressions to estimate the BLT fitness of C-mutants in the A-condition and A-mutants in the C-condition.

Difference in adaptive mutant fitness between conditions. Mutant's fitness were called as significantly different between A and C-conditions if the two 95% confidence intervals did not overlap. We discovered 178 such clones (108 A-mutants and 70 C-mutants), all of which were adaptive in both environments.

Possible reasons for the slight discrepancy between BLT and competitive fitness estimates. We can think of at least three possible reasons for this discrepancy. One possible reason is that we use a different set of reference lineages in the BLT experiments and competition assays. It is possible, for example, that some of the lineages that we use as reference in the competition assay are not in fact neutral in one or both of the conditions.

Another possible reason is that fitness is weakly frequency- dependent (this is expected in batch culture experiments [72]). Frequency dependence can manifest itself in a discrepancy between BLT and competition assays because lineages are present at much

higher frequencies in the competition assays than in the BLT experiments. Specifically, the median frequency of an adapted clone (as defined from the competition analysis) in the competition assay is 4×10^{-4} at the initial time point, whereas the median frequency of an adapted lineage is 3×10^{-6} at the initial time point (the frequency of the adapted mutant driving the lineage frequency must be even lower since many if not most adapted lineage also initially contain non-adapted individuals).

A third possible reason is that the media composition in the BLT experiments and in competition assays could be somewhat different at later stages of the growth cycle because population compositions are different and the media composition is determined by the collective metabolism of all variants present in the population.

Given the overall concordance of fitness estimates, we decided that dissecting these relatively minor effects was not particularly important within the scope of the present work.

4 Genome sequencing and analysis

We sequenced full genomes of 219 A-mutants, 187 C-mutants, 8 non-adapted evolved isolates and 24 ancestral isolates sampled from the inoculum population. Sequencing failed for four A-mutant and six C-mutants, leaving us with 215 A-mutants and 181 C-mutants with sequenced genomes, 8 non-adapted evolved isolates and 24 ancestral isolates (a total of 428 clones). For all remaining clones, we obtained high quality genome data ($>$ 4x coverage, mean coverage of 24x).

4.1 DNA extraction and library preparation and sequencing

DNA was extracted using a modified variant of the YeaStar yeast genomic DNA extraction kit Protocol I (Zymo research #D2002). In particular, a number of solutions were produced in-house, including YD Digestion buffer (1% SDS + 50mM Na_2PO_4), DNA Wash buffer (80% ethanol + 20mM NaCl) and Elution Buffer (10mM Tris-HCl). 0.2ul of 25mg/mL RNAse A (Zymo research #E1008-8) was used for each sample, as well as 1 Unit (0.2μL of 5U/μL stock solution) of Zymolyase (Zymo research #E1004).

Libraries were prepared using the method described in Ref. [65] and sequenced on the Illumina HiSeq4000 platform. Sequencing services were provided by Novogene Inc. and the UCSD Institute for Genomic Medicine.

4.2 Identification of new mutations

4.2.1 Small Variant calling

Reads were first trimmed using Trimmomatic with parameters

```
HEADCROP:10
ILLUMINACLIP:NexteraPE-PE.fa:2:30:10
LEADING:3
TRAILING:3
SLIDINGWINDOW:4:15
MINLEN:36
```

Reads were then mapped with bowtie2 (v. 2.3.4.3) using `-sensitive` parameters to the *Saccharomyces cerevisiae* reference genome (v. R64-2-1) with the addition of an extra "chromosome" defining the barcode locus. Reads were sorted, duplicates marked and short variants were called and filtered using GATK (v. 4.0.11.0) AddOrReplaceReadGroups, MarkDuplicates, HaplotypeCaller and VariantFiltration, respectively. Variant filtration used the filter expression

```
QD<10.0 || FS>20.0 || MQ<20.0 || AN>10 || AF<0.25 || QUAL<100.0 || DP<3
```

All other commands used default parameters. Variants were annotated with ENSEMBL Variant Effect Predictor using their command-line tool. As many variants had multiple possible annotations, coding sequence annotations ("missense_variant", "frameshift_variant", "stop_gained" and "stop_lost") were prioritized over synonymous annotations, which were prioritized over upstream noncoding annotations (within 2kb of a gene) and finally downstream noncoding annotations (again within 2kb of a gene). Variants further of 2kb of any gene or those within 2kb but with no annotations were removed as likely nonfunctional. Finally, variants with less than 3 reads of support for the derived allele were removed as putative false positives.

Additional filtering to remove erroneous and ancestral variants. The procedure described above identified 34,720 small variants across 428 sequenced isolates. We expect that many of these variants are sequencing and/or mapping errors that our procedure failed to remove, as well as fixed differences from the reference genome present in the ancestor of our experiment. To further filter out such spurious variants, we estimate the ancestral allele frequency spectrum from 24 sequenced ancestral clones and compare it with a typical allele frequency spectrum of 24 adapted mutants (averaged over 1000 random draws of 24 adapted mutants). As Figure S12 shows, the latter has an excess of variants that are present only in one clone, as expected for *de novo* mutations. The fact that there is no excess of mutations present in two or more adapted clones suggests that all or most mutations observed in two or more adapted clones are not adaptive. After removing 303 such variants, each of which was detected in 110 isolates on average, we are left with 1842 mutations across 428 sequenced strains (4.30 per clone), of which 33 strains carry no detectable derived small variants (Table S1 and Data S2).

4.2.2 Copy number variant calling

To identify large copy number variants (CNVs), we generate coverage plots for each sequenced clone by averaging read depth into 1kb windows with `bedtools genomecov`. An example plot is shown in Figure S10A. As coverage negatively correlates with the distance to telomeres (Figure S11), we re-calculate coverage after correcting for this variation (Figure S10B). We then manually identify CNVs from these corrected coverage plots by visualizing the coverage distribution at higher resolution (Figure S10C).

4.3 Identification of driver loci carrying small adaptive mutations

To differentiate adaptive "driver" mutations among residual ancestral and erroneous variants as well as nonadaptive "passenger" mutations, we rely on the idea of genetic parallelism, i.e., the fact that loci under selection gain mutations in independent lineages more often than expected by chance [23, 26]. We follow a similar procedure to the method described in Ref. [26]. For each gene, we define its *multiplicity* as the number of clones that carry a mutation in this gene. Since shorter genes require lower multiplicity to be called adaptive, we bin genes by their length into six 1kb bins plus one bin for genes with length $\geq$ 6kb. For each length bin $\ell = 1, 2, \ldots, 7$, we count the number of genes whose multiplicity is $m = 1, 2, \ldots$, denoting these counts by $k_{\ell m}$. We obtain the number of such genes $\langle k_{\ell m} \rangle$ expected in the absence of selection as follows.

We randomly and independently redistribute $N = 1718$ mutations (small mutations in adaptive clones after removing multiple mutations in the same gene in the same clone) across 7226 yeast genes 1000 times, with the probability for each mutation landing in a given gene being proportional to its length + 2kb. Then, the observed excess number of mutations with multiplicity m in length bin ℓ is $a_{\ell m} = \max\left\{0, k_{\ell m} - \langle k_{\ell m} \rangle\right\}$. These excess mutations are assumed to be adaptive. We then redistribute the remaining $\lfloor N - \sum_{\ell=1}^{7} \sum_m a_{\ell m} \rfloor$ potentially non-adaptive mutations as before, and identify additional excess mutations as adaptive. We repeat this procedure iteratively until the total number excess mutations is ≤ 1. We achieve convergence after 8 iterations and thereby obtain the final expected counts $\langle k_{\ell m} \rangle$.

Next, we would like to identify specific loci that carry adaptive mutations as those with multiplicities above some threshold. Specifically, we would like to determine multiplicity thresholds M_ℓ for each length bin $\ell = 1, \ldots, 7$, so that all loci in that bin with multiplicities $\geq M_\ell$ are called adaptive. To do so, for all ℓ we calculate the expected FDR at the given multiplicity threshold M_ℓ as

$$\beta(M_\ell) = \frac{\sum_{m \geq M_\ell} \langle k_{\ell m} \rangle}{\sum_{m' \geq M_\ell} k_{\ell m'}}.$$

We choose the multiplicity thresholds M_ℓ, so that $\beta(M_\ell) \leq \beta^*$ for all ℓ and for some desired β^*. We use $\beta^* = 10\%$.

We estimate the overall FDR as

$$\beta = \frac{\sum_{\ell=1}^{7} \sum_{m \geq M_\ell} \langle k_{\ell m} \rangle}{\sum_{\ell'=1}^{7} \sum_{m' \geq M_{\ell'}} k_{\ell' m'}}.$$

We conduct this analysis considering all 396 sequenced adaptive isolates together, as well as A- and C-mutants separately. Loci identified in any one of these three analyses are defined as putative adaptive loci. After identifying putative adaptive loci this way, we assume that all discovered mutations in these loci are adaptive (Data S3). We confirm that there is an excess of small adaptive mutations in adapted isolates when compared to ancestral isolates (Figure S13B).

4.4 Probability of genetic parallelism

We calculate the probability of genetic parallelism P_g for a set of mutants as follows. We consider every pair of mutants, and calculate the proportion that have a mutation in at least one common adaptive locus (including both small variants and CNVs). Adaptive isolates with no mutations at the identified adaptive loci are assumed to have an adaptive mutation at a locus that is not shared with any other isolate in the set.

To test whether A- and C-mutants have different probabilities of genetic parallelism, we reshuffle the evolution treatment label (i.e. Alone vs Community) across all A- and C-mutants and calculate P_g for both resulting groups. We obtain the absolute value of the difference in P_g between the two groups, $|\Delta P_g|$, in 1000 such permutations, and estimate the P-value as the fraction of permutations where $|\Delta P_g|$ exceeds the observed difference. We find that $P = 0.06$, suggesting that there is no significant difference in the probabilities of genetic parallelism between A- and C-mutants.

4.5 Results

Small mutations. The distributions of derived small variants per clone is shown in Figure S13A and their summary statistics are given in Table S1. These data show that the majority of small variants detected in the evolved clones are still likely ancestral or erroneous. We can estimate the expected number of adaptive small variants as follows. A typical adapted isolate carries 1.18 more mutations compared to an ancestral isolate (Figures S12, S13, Table S1). However, not all of these mutations may be adaptive. Indeed, given that small indels and single-nucleotide mutations occur at rate 3×10^{-3} per genome per generation [69], we expect 0.18 of such mutations to have occurred on the line of descent of any isolate sampled at cycle 9 ($\sim$ 60 generations). Based on this estimate, a typical adapted clone is expected to carry 1.18 - 0.18 = 1.00 adaptive mutation.

One potential problem with this estimate is that our yeast strain may have a somewhat different mutation rate than the strain used in Ref. [69]. We can obtain an alternative estimate for the number of adaptive mutations per clone by comparing adapted clones

with the neutral ones. We find that a typical neutral clone carries 1.96 ± 0.88 more mutations than a typical ancestral isolate[1] (Table S1), which is greater than 1.18 extra mutations carried by a typical adapted clone. Thus, it is possible that a typical adapted clone carries no beneficial small mutations.

The problem with the second estimate is that some of the clones identified as neutral may in fact carry adaptive mutations[2]. Therefore, we use both methods to obtain bounds on the number of adaptive mutations carried by a typical adapted clone and conclude that a typical adapted clone is expected to carry between 0 and 1 small adaptive mutations. Carrying out the same calculations for the A- and C-mutants separately, we estimate that a typical A-mutant carries between 0 and 1.34 small adaptive mutations (so that between 0 and 288 out of 1008 small mutations found in A-mutants are expected to be adaptive), and a typical C-mutant carries between 0 and 0.61 small adaptive mutations (so that between 0 and 110 out of 717 small mutations found in C-mutants are expected to be adaptive; Table S1).

Using genetic parallelism, we identify 185 mutations at 63 loci as adaptive (on average 0.47 mutations per clone), consistent with our expectation. 76 of these mutations at 39 loci are found in 60 A-mutants (on average 0.35 mutations per clone) and 109 mutations at 56 loci are found in 81 C-mutants (on average 0.60 mutations per clone; Table S1).

Large CNVs. We identified 176 CNVs across 167 strains (Data S2), of which 85 are aneuploidies. The distribution of CNVs per clone is shown in Figure S13C and summary statistics are given in Table S1. These data show that none of the ancestral or neutral isolates carry CNVs and that most adapted clones carry zero or one such mutation.

Since we found no CNV events in 32 sequenced ancestral and neutral isolates (Figure S13C, Table S1), we estimate the frequency of observing a non-adaptive CNV event as at most 1/32. Thus, we expect at most 12.4 such events among 396 sequenced adaptive clones. In fact, we found 176 CNV events, which suggests that all or almost all of them are adaptive (expected FDR ≤ 0.07; Data S3).

We found no statistical relationship between the number of CNV mutations and the number of identified small mutations per isolate ($R = -0.07$, $P = 0.18$).

Total number of identified adaptive mutations per clone. After combining small mutations and CNVs together, we find that a typical A-mutant carries 0.74 identified adaptive mutations with 100 A-mutants having no identified adaptive mutations (Figure S14 and Data S2). A typical C-mutant carries 1.11 identified adaptive mutations with 46 C-mutants having no identified adaptive mutations (Figure S14 and Data S2). Since all A- and C-mutants gained fitness in their home environment, each of them must

[1]This number is larger than 0.18 expected based on the yeast mutation rate, but the difference is not statistically significant ($P = 0.08$, t-test, expected $\mu = 0.18$).

[2]This is confirmed by the fact that we find two mutations at driver loci in the neutral clones (see Figure S13 and Table S1).

have at least one adaptive mutation. Therefore, the "unknown" sectors in Figure 1C in the main text refers to the numbers of A- or C-mutants without any identified adaptive mutations.

Pre-existing mutations. We use genetic information to test for the prevalence of preexisting mutations of type II, i.e., those that arose prior to the integration of the DNA barcodes, so that multiple lineages may carry an adaptive mutation identical by descent. If such mutations were prevalent, we would expect to observe an excess of adapted clones carrying identical genetic mutations, compared to ancestral isolates.

CNV events are not suitable for this analysis because they occur at very high rates. Indeed, many CNVs are aneuploidies, which occur at rate 9.7×10^{-4} per generation [69]. The only consistent segmental CNVs are ChrIV-1n and ChrIV-3n. ChrIV-1n mutations are localized to identical breakpoints across 64 mutants. However, these breakpoints are concordant with highly similar repetitive regions, YDRWTy2-2/YDRCTy1-2 and YDRWTy2-3/YDRCTy1-3. There are three different classes of ChrIV-3n amplifications across 10 mutants. At least some of these breakpoints also appear to be localized close to known repetitive regions, including YDRCTy2-1, YDRCTy1-1 and YDRWTy2-2. Thus, we suspect that these recombination-driven segmental events also occur at high rates and are not necessarily indicative of pre-existing variation.

As mentioned above, we find no excess of identical small mutations present in multiple adapted clones (Figure S12). In fact, an identical small mutation is found less frequently in multiple adapted clones than in multiple ancestral clones, suggesting that some of the pre-existing genetic variation may have been deleterious.

5 Simulations of evolutionary dynamics and the estimation of rates of adaptive mutations

We found that the sets of A- and C-mutants are genetically distinct (Figures 1D in the main text, S14 and Data S3), despite all of them being more fit than the ancestor in both environments. In this section, we show that this somewhat puzzling observation can be explained by the differences in the evolutionary dynamics in the concurrent mutation regime [73].

There are two key differences between the A- and C-conditions. First, the bDFEs are different (Figure 1A in the main text), resulting in different increases of population's mean fitness over time. Second, the fitness rank orders of adaptive mutations are also different (Figure 1A,B in the main text). These two facts imply that in the concurrent mutation regime the chances for a given mutation to escape drift while rare and reach a certain frequency and be sampled can be substantially different in the two conditions. Next, we develop a quantitative version of this argument.

As described in Section 4, we classify all discovered adaptive mutations into mutation classes by the type of CNV or the gene in or near which the mutation occurred (Data S3). Let k_{im}^A and k_{im}^C be the number of sequenced A- or C-mutants that carry a mutation from class m sampled from the replicate population $i = 1, 2, 3, 4, 5$ (see Table S2). We would like to know whether the differences between k_{im}^A and k_{im}^C can be explained by the observed differences in the bDFEs and by differences in the fitness benefits provided by mutations of class m in the A- and C-conditions.

The challenge is that the probability $\Pr\{k; s, U\}$ of observing k mutants of a certain type in a sample from a given population depends not only on the selection coefficients s of adaptive mutations of this type (which we have measured, as described in Section 3) but also on the unknown rate U at which such mutations arise. Therefore, we first find the mutation rates that fit our data and confirm that these rates are biologically plausible. We then ask how well the expected numbers of A- and C-mutants carrying specific mutations match the observed numbers k_{im}^A and k_{im}^C, given the estimated mutation rates.

5.1 Data

Exclusion of pre-existing mutations. A number of lineages are identified as adapted in multiple populations, indicative of pre-existing mutations of type I (see Section 2.6.2 for more details). Since such mutations do not carry information about the mutation rate, we exclude them from this analysis. That is, numbers k_{im}^A, k_{im}^C given in Table S2 and in Figure S16 are the numbers of sampled and sequenced clones with unique barcodes.

Selection coefficients. Fitness of individual mutants in the BLT experiments are estimated based on the competition assay data, as described above (see Section 3.4), and selection coefficients s_m^A and s_m^C are taken as averages over all mutants carrying a mutation from a given mutation class (Table S2).

Mean fitness trajectories. Our model described below takes into account the fact that the probability of a newly arisen beneficial mutation to survive genetic drift depends on how the mean fitness of the population changes over time. Thus, when simulating the evolutionary dynamics, we use the empirical mean selection coefficient trajectories $\bar{s}^A(t)$ and $\bar{s}^C(t)$ in the A- and C-conditions, respectively. $\bar{s}^A(t)$ and $\bar{s}^C(t)$ are computed by first averaging the values of the mean selection coefficient (estimated in as described in Section 2.6.2) over all five replicates and then fitting the logistic function to these data points (see Figure S4B).

5.2 Model

To keep the model as simple as possible, we assume that our population has the constant size $N = 2 \times 10^6$ in both A- and C-conditions, mutations from the mutation class m arise at (an unknown) rate U_m per division in both conditions. We assume that all mutation from class m confer the same (known) fitness benefits s_m^A and s_m^B relative to the ancestor in the A- and C-condition, respectively (Table S2. We also assume that all mutants are sampled at time $T = 60$ generations after the beginning of the experiments in both A- and C-conditions, which roughly corresponds to cycle 9, assuming $\log_2 100 = 6.64$ doublings per cycle (see Section 2.3).

To estimate the mutation rate U_m for mutation class m we define the log-likelihood function

$$L(U_m) = \frac{1}{5}\sum_{i=1}^{5} \log \Pr\left\{k_{im}^A; s_m^A, U_m\right\} + \frac{1}{5}\sum_{i=1}^{5} \log \Pr\left\{k_{im}^C; s_m^C, U_m\right\}. \tag{2}$$

The sampling probability $\Pr\{k; s, U\}$ depends on the number of lineages that independently arose in the population and that carry a mutation of the focal type, as well as on the frequencies of these lineages at the sampling time point T. It is difficult to obtain an analytical expression for this probability because it requires integrating over all these nuisance parameters. We therefore compute the sampling probability numerically, using population dynamic simulations described below.

5.2.1 Evolutionary dynamics simulations and the estimation of the sampling probability

As mentioned above, difference in the bDFE between the A- and C-conditions may contribute to the observed differences in the genetic composition of sampled mutants. The bDFE indirectly affects the survival probability of a newly arisen beneficial mutation by altering how the mean fitness of the population changes over time. Thus, we design our simulations so that they match the average empirical mean selection coefficient trajectories in the A- or C-condition (see Section 2.6.2 and Figure S4B). Matching these trajectories in simulations of the full Wright-Fisher where all mutation classes segregate simultaneously is difficult. Instead, we simulate the arrival and spread of mutations of each mutation class separately, while accounting for changes in mean fitness using our logistic fit of the observed mean fitness trajectories (Figure S4B). This approach also allows us to use branching process approximations described below in Section 5.2.2, which greatly speed up the calculations.

Since in this section we are concerned with mutants of one mutational class in one environment, we omit the subscript m and superscripts A/C. In other words, we assume that the mutations arrive at rate U per individual per generation and have selection coefficient s, and we sample 88 mutants from this population at time point $T = 60$.

In our simulations, we allow for new mutations to arise between 1 cycle prior to the beginning of the experiment up to cycle 9. Thus, we divide the time interval between -6.6 and $T = 60$ generations into 260 to 1300 segments of length $\Delta t = 0.01/s$ generations. For each time segment $(t_i, t_i + \Delta t)$, we draw the number of new mutants arising in the population in that segment from the Poisson distribution with rate $N\,U\,\Delta t$. Each of these mutants survives until the sampling time point T with probability $P_{\text{surv}}(T; s, t_i)$, given by equation (3) below. For each mutant that survives, we draw its establishment time τ from the distribution given by equation (4) below. We then set the mutant's frequency at the sampling time point to $n(T; s_m, \tau)/N$, where n is given by equation (5) below. At the end of each simulation run, we obtain a list of frequencies of all independently arisen mutants carrying mutation of type m. We assume that each independently arisen mutants is linked to a distinct barcode. We then randomly sample 88 clones from the whole population and discard those that do not carry the focal adaptive mutation. If multiple clones are sampled from the same lineage, only one is retained. We further randomly sub-sample these clones with 97.5% success probability, simulating the small whole-genome sequencing failure rate, which results in the final number k of sampled clones that carry a mutation from the focal mutation class. We estimate the probability of sampling k clones, $\Pr\{k; s, U\}$, by running 10^4 simulations and recording the fractions of simulations where we observe k sampled clones.

5.2.2 Branching process approximations for mutant growth dynamics

Consider a mutant that arises at some point $t_0 < T$ on the ancestral background. The early population dynamics of such mutant lineage can be modeled as a branching process [73]. In particular, Desai and Fisher [73] used the branching process approximation to derive the probability that a mutant with selection coefficient s that arose at time zero in the ancestral population (i.e., whose mean selection coefficient is zero) has not gone extinct by time t and the related probability that the mutant "establishes" at time τ (see equations (11) and (17) in Ref. [73]). However, this model ignores the fact that the mean fitness of the population is changing over time while the focal mutant is still at low frequency. In our experiment, mean fitness changes very rapidly, as can be seen in Figure S4B, which can significantly alter mutant's survival probability and its establishment time. Assuming that the mean selection coefficient trajectory $\bar{s}(t)$ is known (see Section 5.1), we can model mutant dynamics analogous to Ref. [73] but with a generalized birth-death model with growth rate $1 + s - \bar{s}(t)$ and death rate 1. In this model, the probability that a mutant that arose at time t_0 survives until time t is given by

$$P_{\text{surv}}(t; s, t_0) = \frac{\omega(t_0)}{1 + \omega(t_0) - e^{-\rho(t, t_0)}}, \tag{3}$$

where

$$\begin{aligned}\omega(t) &= s - \bar{s}(t),\\ \rho(t,t_0) &= \int_{t_0}^{t} \omega(t')\,dt',\end{aligned}$$

provided that $\omega(t_0) > 0$. Conditional on surviving, the probability that this mutant establishes at time τ is given by

$$P_{\text{est}}(\tau; s, t_0) = \frac{\omega(t_0)}{1+\omega(t_0)}\ \exp\left[-\rho(\tau,t_0) - \frac{e^{-\rho(\tau,t_0)}}{1+\omega(t_0)}\right]. \tag{4}$$

Once the mutant establishes at time τ and provided that it is still beneficial, i.e., $\omega(\tau) > 0$, its subsequent dynamics are essentially deterministic, so that its size $n(t;\tau)$ at time t is approximately given by

$$n(t; s, \tau) = \frac{e^{\rho(t,\tau)}}{\omega(\tau)}, \tag{5}$$

which is analogous to equation (14) in Ref. [73] in the limit $t \gg 1/s$.

5.2.3 Estimation of mutation rates by maximum likelihood

For each mutation class m, we compute the likelihood function $L(U_m)$ using equation (2) for 40 discrete values of $u_m = \log_{10} U_m$ between -7 and -3 and interpolate between them using a polynomial of degree 4. The likelihood function for chrIII-3n mutations is shown as an example in Figure S15. We find the maximum of this function as a point where the polynomial approximation of L has a zero first derivative with respect to u_m. We estimate the standard error (SE) as the inverse of the square root of Fisher information [74].

5.3 Results

We estimated the rates of driver mutations at 9 loci that were mutated in at least five adapted clones, after excluding gene NUM1 where all mutations are likely pre-existing (see Figure S14, Table S2 and Data S3). Our estimates are generally consistent with those derived from a published mutation accumulation experiment by Zhu et al [69]. In particular, our estimate of the rate of small adaptive mutations in genes HEM1 and HEM2 is $\sim 3 \times 10^{-7}$ per generation, consistent with per basepair mutation rate of 1.67×10^{-10} estimated by Zhu et al [69]. Gene YIL169C is an exception, with an estimated rate of adaptive point mutations of 7.76×10^{-6} per generation. We estimate the rates of large CNV events to be $\sim 10^{-5}$ per generation, again consistent with the genome-wide rate of aneuploidies of 1.04×10^{-4} estimated by Zhu et al [69]. Our estimate of the segmental

duplications ChrIV-3n is much lower (3.24×10^{-7} per generation), also consistent with Ref. [69], although they do not provide a quantitative estimate of such events.

The probability that at least one sequenced mutant from all five replicate populations has a mutation with a given selection coefficient s and mutation rate U is shown in Figure S16A, for both A- and C-conditions. As expected, this function is different between conditions because the mean fitness dynamics are different (Figure S4B). Finally, we directly compare the observed numbers of mutations of each mutation class with the expected numbers in the A- and C-conditions and find a reasonable match (Figure S16B).

6 Phenotyping

We selected 31 C-mutants and 28 A-mutants for three types of phenotyping experiments: measurements of yields in the community, microscopy for detecting possible physical associations between yeast and algae, and growth-curve measurements of individual mutants in the A-condition. We selected these 59 mutants manually to cover a diversity of mutations and fitness values represented in the sampled adaptive mutants (see Data S3 for the number of mutants selected from each mutation class). Our reasoning for this selection rather sampling randomly is that mutants carrying the same driver mutation would have similar phenotypic values[3]. Then, by selecting clones for phenotyping randomly, we would not observe rare phenotypes. To account for this over-dispersion in the selection of mutants we apply the mutation weighting procedure described below in Section 6.4.

6.1 Measurements of species yields in mutant communities

We create mutants communities as follows. On day 0, we inoculate 50mL growth media (in 250mL non-baffled Erlenmeyer flask) with 1mL of CC1690 *C. reinhardtii* stock stored in a liquid nitrogen freezer and incubate for 20 days in our standard conditions. On day 20, 100µL of this culture are transferred to the BLT experiment conditions (10mL of fresh media in a 50mL flask). Also on day 20, the 60 yeast strains (including the ancestor) are individually inoculated into the evolution condition from frozen stocks. On day 25, we form the mutant communities by transferring 100µL of each yeast culture and 200µL of the algae culture into fresh media (200µL of alga were used instead of 100µL because the density of algae culture was approximately 50% of that at the initiation of the evolution experiment). These mutant communities are grown for one cycle in our standard conditions. On day 30, we transfer 100µL of each mutant community into 10mL fresh

[3]This hypothesis was indeed confirmed. We tested whether mutants carrying the same mutation have more similar yeast and alga yields, r and K values than random mutants. We carried out these tests for the 9 clones with chrIII-3n mutations, 5 clones with the chrIV-3n mutations, 3 clones with the chrIV-1n mutations, 3 clones with HEM2 mutations and 3 clones with HEM3 mutations. In all cases, clones carrying the same mutation had more similar phenotypes than random mutants, but in most cases the difference was not statistically significant, presumably due to lack of power.

media, as in the BLT experiment. We estimate both yeast and alga density on day 35, as follows. We estimate alga density by measuring chlorophyll b fluorescence. To that end, we transfer 200µL of each culture into a well of a black-wall clear-bottom 96-well plate (Corning) and measure fluorescence in a plate reader (Molecular Devices Spectramax i3x, excitation at 435nm and observation at 670nm). To measure yeast density, we dilute the culture 1:1600, plate 100µL on Petri dishes with standard media + 1% agarose, grow at 30°C for 3 days and count colonies.

Yield estimates can be found in Data S1. Replicate measurements show reasonably good correlation (Figure S17). We find a positive correlation between Alga yield and yeast mutant fitness in both the A- and C-conditions (Figure S18).

6.2 Microscopy

To detect potential physical associations between algae and beneficial yeast mutants, we created mutant communities as described in Section 6.1. Communities were mounted on glass microscope slides (Fisher Scientific 12550143), sealed with Dow Corning high vacuum grease (Amazon B001UHMNW0) and imaged on a light microscope using a 20x objective with DIC. Figure S20 shows one representative community, the remaining 17 imaged mutants along with WT controls can be found in the Dryad data repository.

6.3 Mutant growth curve measurements

To estimate the growth parameters r and K for individual beneficial mutants, we carried out growth curve measurement experiments of individual yeast mutants and the ancestor in the A-condition. To this end, we inoculated all 60 yeast strains (including the ancestor) individually into the BLT condition (10mL of media in 50mL flasks) from frozen stocks and propagated them for two cycles (10 days). During the third cycle, we estimated yeast densities on days 10, 10.5, 11, 11.5, 12, 13, 14 and 15 by plating and colony counting as described in Section 6.1. The growth curves are shown in Figure S21 and the data are provided in Data S1.

We estimate r as the slope of the relationship between $\log(\text{CFU/mL})$ and time (in hours) for the three measurements between 12 and 36 hours of growth. We estimate K as the maximum observed density (in CFU/mL). r and K estimates can be found in Data S1. Growth rate estimates are well correlated between replicates (Figure S22A). K measurements are more noisy (Figure S22B). The relationship between these growth parameters, mutant fitness and species yields in mutant communities are shown in Figure 3 in the main text and Figure S23.

6.4 Statistical analysis

Mutation weighting. Even though not all A- or C-mutants were phenotyped, we would like to make certain statistical statements about the distribution of phenotypes among all sampled A- or C-mutants. We can do so by weighting each phenotyped mutant according to its mutational class. We do so as follows. First, we associate each of the 59 phenotyped mutants with a single driver mutation. Mutants with multiple driver mutations are associated only with the driver mutation from the most common mutational class. Mutants with no identified driver mutations are associated with a unique unknown mutations. Then, for each of the phenotyped mutants, we weight its measured phenotypic value by the number of A- or C-mutants that share a mutation class with it, divided by the number of phenotyped A- or C-mutants that share a mutation class with it. Based on this reweighted distribution of phenotypes, we calculate various statistics such as kernel density estimates, correlation between phenotypes and probabilities of parallelism (see below).

Kernel density estimation. We use kernel density estimate (KDE) to determine how likely certain phenotypic trait values would occur among random A- and/or C-mutants. Specifically, we obtain the kernel density estimates $D_A(y, a)$ and $D_C(y, a)$ for the probabilities that a community formed by algae and a random A- or C-mutant, respectively, would produce a yeast yield y and alga yield a. To estimate D_A, we apply the `kde2d` function in R with bandwidth 1 along the x-axis and 4/3 along the y-axis to the mutation-weighted yield data for the A-mutants. We analogously obtain $D_C(y, a)$.

Accounting for measurement errors in statistical tests. As the measurement errors in our estimates of phenotypic values (r, K, yeast yield and algae yield) are quite large, we use a permutation and resampling procedure to determine the statistical significance in various tests involving these variables. In this procedure, we permute isolate labels and resample the phenotypic values associated with each isolate from the normal distribution with the estimated mean and with the standard deviation set to the estimated standard error of the mean. We carry out 1000 permutation and resampling instances in each test.

Phenotypic parallelism analysis. We quantify the degree of parallelism among a set of mutants with respect to a pair of quantitative traits X and Y by estimating the probability that, for two randomly selected mutants, trait X changes in the same direction in both mutants and trait Y changes in the same direction in both mutants. Mathematically, if one randomly selected mutant has trait increments ΔX_i and ΔY_i relative to the ancestor and the other mutant has trait increments ΔX_j and ΔY_j, we estimate the probability that both $(\Delta X_i)(\Delta X_j) \geq 0$ and $(\Delta Y_i)(\Delta Y_j) \geq 0$. This measure of phenotypic parallelism emphasizes the direction of change rather than the magnitude, which,

we believe, is more meaningful than some other quantitative measures, at least for the community and growth phenotypes that we consider in this study. When we compute this measure for the pair of yields of mutant communities, in which case X and Y are yeast and alga yields, we refer to it as the probability of ecological parallelism, P_{e}. When we compute this measure for the growth phenotypes, in which case X and Y are r and K, we refer to it as the probability of phenotypic parallelism, P_{ph}.

We obtain these probabilities of parallelism for the A- and C-mutants after applying the mutation weighting procedure described above. To determine the statistical significance of the difference between the probabilities of parallelism for the A- and C-mutants, we resample the phenotypic values of each of the 59 mutants from the normal distribution (see above) and permute mutant genotype and home-environment labels, so that the genotype and label are always associated with each other but dissociated from the phenotypic values. We then calculate the parallelism probabilities for these permuted and resampled data. We estimate the P-value by carrying out this permutation and resampling procedure 1000 times.

7 Possible function effects of mutations in *HEM1*, *HEM2* and *HEM3* genes

Three critical components of the heme biosynthesis pathway, HEM1, HEM2 and HEM3 are putative targets of adaptation in this study, and provide a substantially larger fitness benefit in the C-condition than in the A-condition (see Data S2 and Data S3). Most mutations found in these genes probably compromise the function of the encoded enzymes and lead to a decreased "siphoning" of succinyl-coenzyme A (sCoA) from the TCA cycle and the production of less heme and/or decoupling of aerobic-driven regulation from aspects of central metabolism. Although yeast is already capable of performing fermentation under ambient oxygen concentration, we speculate that these mutations enables yeast to ferment under even higher oxygen concentrations that results from alga photosynthesis.

7.1 HEM1

HEM1 encodes the mitochondrial 5-aminolevulinate synthase (ALAS) that catalyzes the first committed step of porphyrin through the condensation of glycine and sCoA using the cofactor pyridoxal 5'-phosphate (PLP):

$$\mathrm{sCoA} + \mathrm{glycine} + \mathrm{PLPcofactor} \rightleftharpoons \text{5-aminolevulinate} + \mathrm{CoA} + \mathrm{CO_2} + \mathrm{PLPcofactor}$$

ALAS links heme/cytochrome production with the TCA cycle and aerobic respiration via sCoA, and thus plays a key role in cellular energetics [75]. ALAS functions as a homodimer

(with subunits referred to as A and B below). A crystal structure of *S. cerevisiae* HEM1 is available (https://www.rcsb.org/3d-view/5TXR/1).

We found 5 adaptive mutations in the *HEM1* gene, four of which occurred in the C-mutants (Data S2 and Data S3). A nonsense mutation at residue 166 (out of 548) in HEM1/ALAS leads to a truncated coding sequence and presumably loss of function. All other mutations alter amino acids that are conserved in all sequenced *S. cerevisiae* strains, which we speculate may also significantly compromise normal HEM1/ALAS function, as described below.

His107Pro mutation does not seem to be involved in any substrate or co-factor binding directly, but a change from histidine to a proline, with significant backbone confirmational constraints may have serious consequences for the folding (and thus function) of the enzyme. Bracketing this position (107) nearby is Arg91, which plays a critical role in sCoA binding, and Asn121, which forms an alpha-carboxylate hydrogen bond with the glycine substrate [76]. Moreover, His107 (of subunit B) forms important structurally stabilizing side-chain interactions with Glu111 (subunit B) and Lys142 (subunit A) (see Figure S3 of [76]), which may very well be disrupted with a proline substitution (lacking a side chain).

Asn152Lys and Asn157Lys mutations occur in a region of the ALAS protein that becomes ordered upon PLP cofactor binding. N152 plays a direct role in coordinating sCoA [76], hydrogen bonding with the carboxylate (COO-) moiety of the sCoA succinyl group. Mutation from asparagine to a positively charged lysine may both disrupt the formation of this hydrogen bond and prevent a key side-chain interaction between Asn152 (subunit A) and Arg91 (subunit B) that stabilizes key structural elements needed for PLP cofactor binding (we expect the side chain of mutation Lys152 to repel that of Arg91 since both are positively charged). Asn157Lys is a few amino acids downstream from Ile153, which also plays a role in carboxylate/sCoA coordination like Asn121 [76]. Asn157 is adjacent to Ile158 (subunit A) that forms stabilizing main-chain and side-chain interactions upon PLP cofactor binding with Asn95 and Asn 97 (both on subunit B); mutation to Lys may disrupt these interactions, along with that of nearby stabilizing interactions between Arg98 (subunit B) and Ala147 (subunit A), due to positive charge repulsion between Arg98 and Asn157Lys (see Figure S3 of [76]).

Gly344Cys mutation occurs at a site that does not directly bind substrate or co-factor but is each bracketed by amino acids that do play key active site roles and could also have structural consequences as conformational flexibility is likely lost with the change away from glycine. Gly344 is flanked (although several amino acids away) by K337 that forms a critical covalent pyridoxyl-lysine bond, and F365 which delineates the sCoA substrate-binding pocket [76]. Gly344 resides on the juncture between a beta-sheet and alpha-helix motif in the protein structure, with little space for a side chain. Mutation of this site

to a cysteine may alter backbone flexibility and the folding of key structural elements. Gly344 is also in close proximity to Cys182 that forms stabilizing hydrogen bonds with amino acids Asn129, Thr275, and Gly 276; having another cysteine nearby may very likely interfere with that hydrogen bonding network.

7.2 HEM2

HEM2 encodes for the cytoplasmic/nuclear, homo-octameric aminolevulinate dehydratase (ALAD; porphobilinogen synthase), which catalyzes the second step in heme biosynthesis:

$$\text{5-aminolevulinate} \rightleftharpoons \text{porphobilinogen} + 2\,H_2O$$

A crystal structure of *S. cerevisiae* HEM2 is also available (https://www.rcsb.org/3d-view/1AW5/1).

We found 5 adaptive mutations in the *HEM2* gene, four of which also occurred in the C-mutants (Data S2 and Data S3). Two frame-shift mutations lead to premature stop codons $\sim$ 100 out of 342 amino acids. The three remaining mutations Ile129Phe, Val132Phe, and Pro264Arg are predicted to have moderate impact.

Ile129 resides on a beta-strand with a side chain embedded in a relatively hydrophobic environment. It is unclear what the consequences of mutation Ile129Phe might be, as phenylalanine is a comparably bulky hydrophobic side chain to isoleucine that would at first glance seem to be a conservative substitution [77]. However, several aromatic amino acids are in the vicinity, including Trp30 and Tyr127; Ile129Phe may form aromatic ring-stacking interactions with these residues to disrupt fold structure.

Val132 is similarly on a beta-strand with a side chain embedded in another nearby hydrophobic pocket and interface with other non-polar amino acids on alpha-helix. The Val132Phe mutation could disrupt the tight packing at this interface as phenylalanine is substantially bulkier than valine. Moreover, Tyr168 is nearby which hydrogen bonds a key water molecule that is hydrogen-bonded to several other backbone atoms flanking Val132; the Val132Phe mutation may also disrupt this by interacting with Tyr168 through aromatic stacking interactions. Pro264 resides in a sharply kinked beta-turn between beta-strand and alpha-helix elements, which may be important for constraining and enabling key interactions of flanking residues with amino acids distributed across different structural elements: Val262/Ser265/Tyr287, Ser265/Glu292, and Lys263/Tyr287 (see https://www.rcsb.org/3d-view/1AW5/1).

Pro264Arg mutation is pronounced not just for the loss of backbone constraint provided by the imino acid proline [77], but it introduces a large positively charged side

change that may form "inappropriate" interactions to disrupt monomer fold and subsequently oligomerization; these include interactions with nearby: negatively charged amino acids: Glu292 and Glu313 aromatic amino acids (through cation-pi interactions) Phe211 (normally interacting with Tyr268 via aromatic stacking), Tyr216 (normally interacting with the backbone of Phe211), Tyr268 (normally interacting with Glu313), and Tyr287 (normally interacting with Lys263 via cation-pi interactions).

7.3 HEM3

HEM3 encodes for the cytoplasmic/nuclear enzyme, porphobilinogen deaminase/hydroxymethylbilane synthase (HMBS), which catalyzes the third step in heme biosynthesis involving four molecules of porphobilinogen to make a linear hydroxymethybilane molecule that looks like a heme/tetrapyrole when "wrapped around":

$$4\,\text{porphobilinogen} + H_2O \rightleftharpoons \text{hydroxymethylbilane} + 4\,NH_3$$

We found 4 adaptive mutations in the *HEM3* gene, three of which occurred in the C-mutants (Data S2 and Data S3). However, since no structure exists for *S. cerevisiae* HEM3 protein and since the homology with the human ortholog for which the structure does exist (https://www.rcsb.org/3d-view/5M6R/1) is rather low ($\sim$ 40% similarity), predicting the functional effects of these mutations is challenging.

8 Supplementary Figures

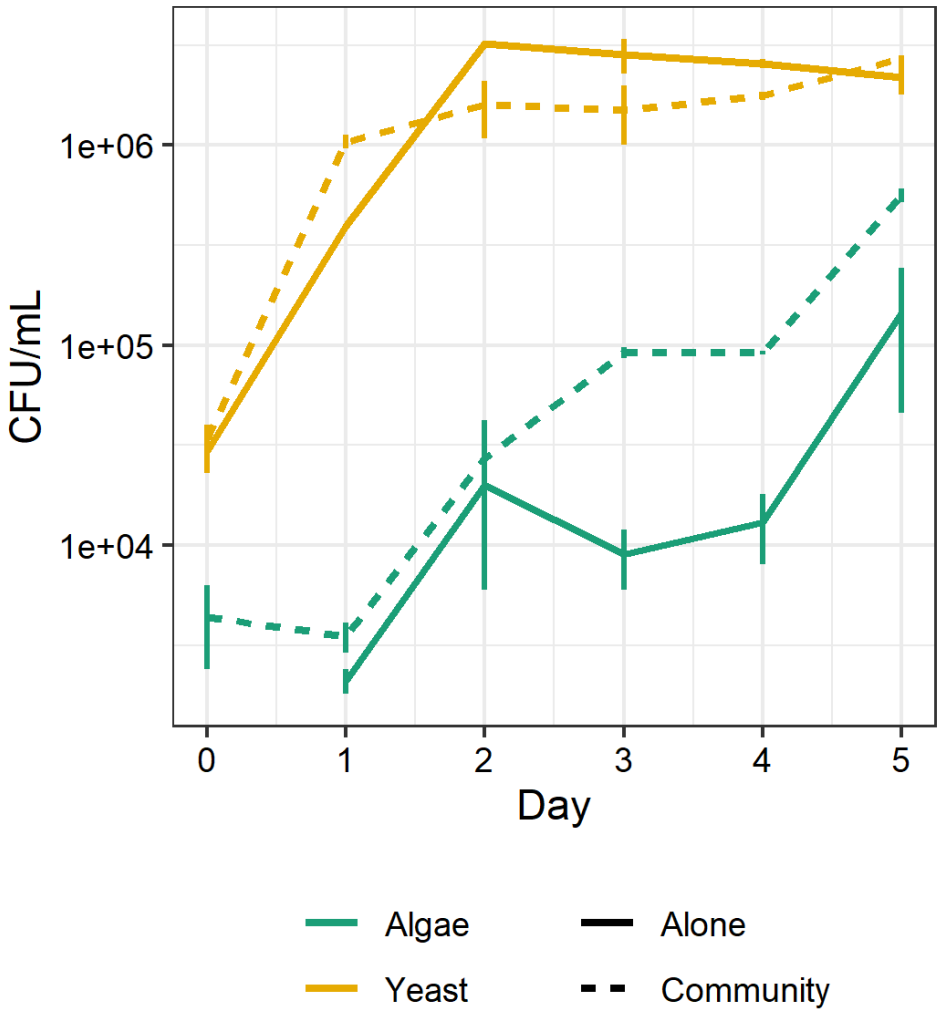

Figure S1. Growth curves for the ancestral strains of the yeast and the alga.

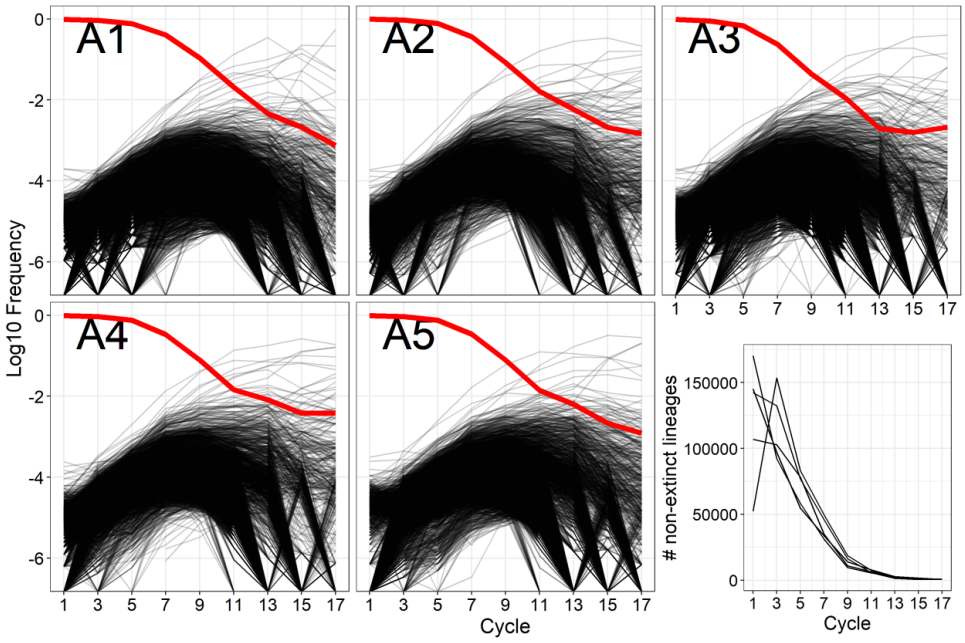

Figure S2. Lineage trajectories in yeast populations in the A-condition. First five panels show individual replicate populations A1 through A5. Barcode lineage frequencies are estimated at every odd cycle. Only the lineages identified as adapted are shown (black lines). Thick red lines show the total frequency of all non-adapted lineages. Last panel shows the number of nonextinct lineages over time for all populations.

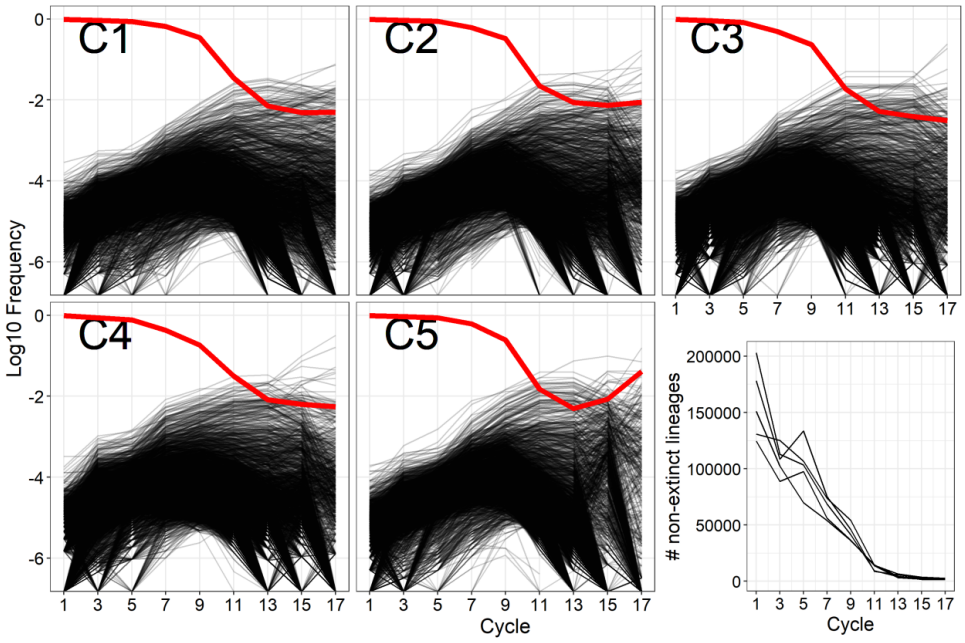

Figure S3. Lineage trajectories in yeast populations in the C-condition. Notations as in Figure S2.

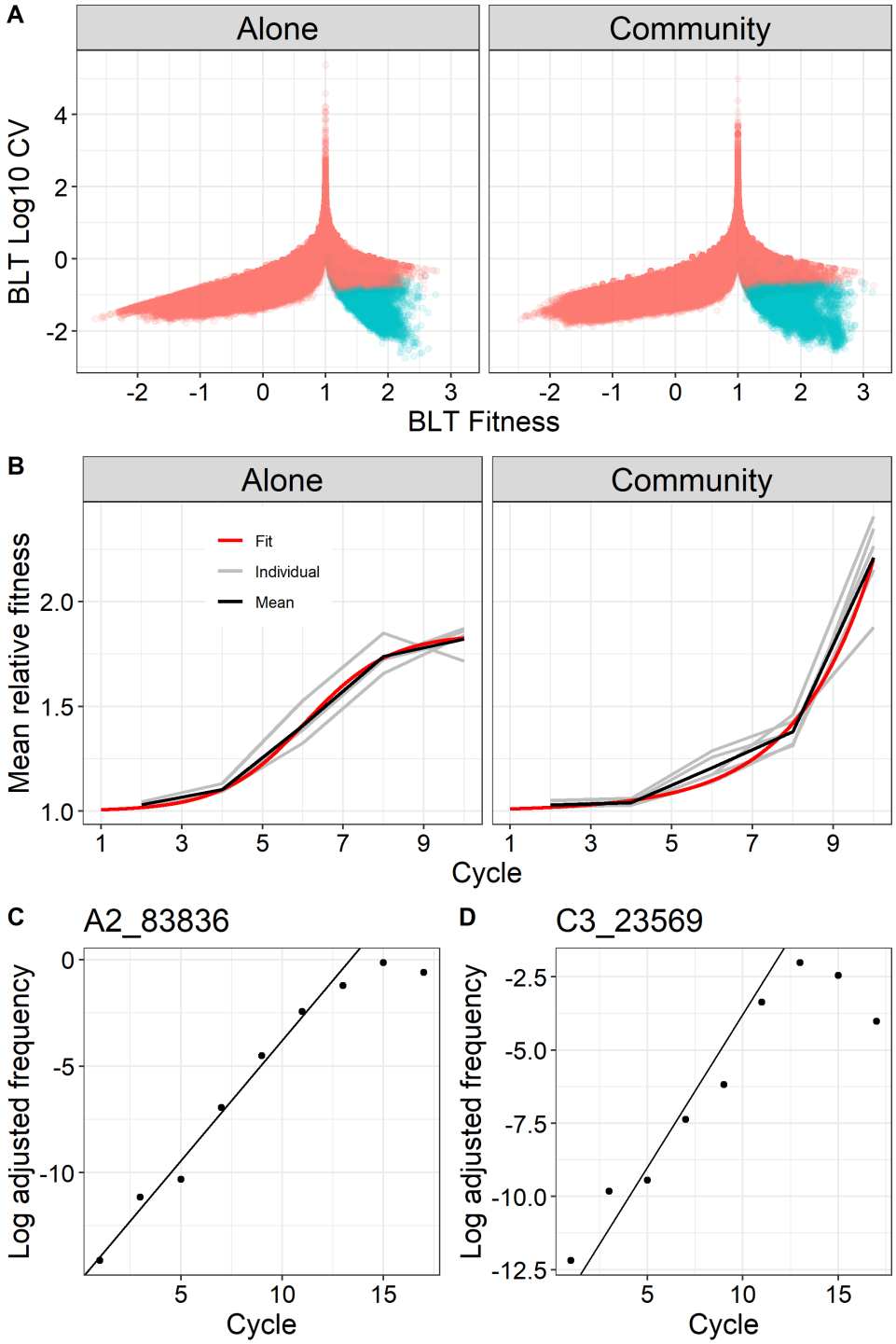

Figure S4. Estimation of fitness of adapted lineages in the BLT data. A. The mean lineage fitness (x-axis) is plotted against the coefficient of variation (CV) of the estimate (y-axis). Blue (red) points indicate lineages identified as adapted (non-adapted). **B.** Mean fitness of each population over time. Individual populations are shown in grey, the average mean fitness trajectory over all populations is shown in black, and a logistic fit to this average trajectory is shown in red. **C, D.** Examples of selection coefficient estimation for one lineage in one A population (C) and one C population (D).

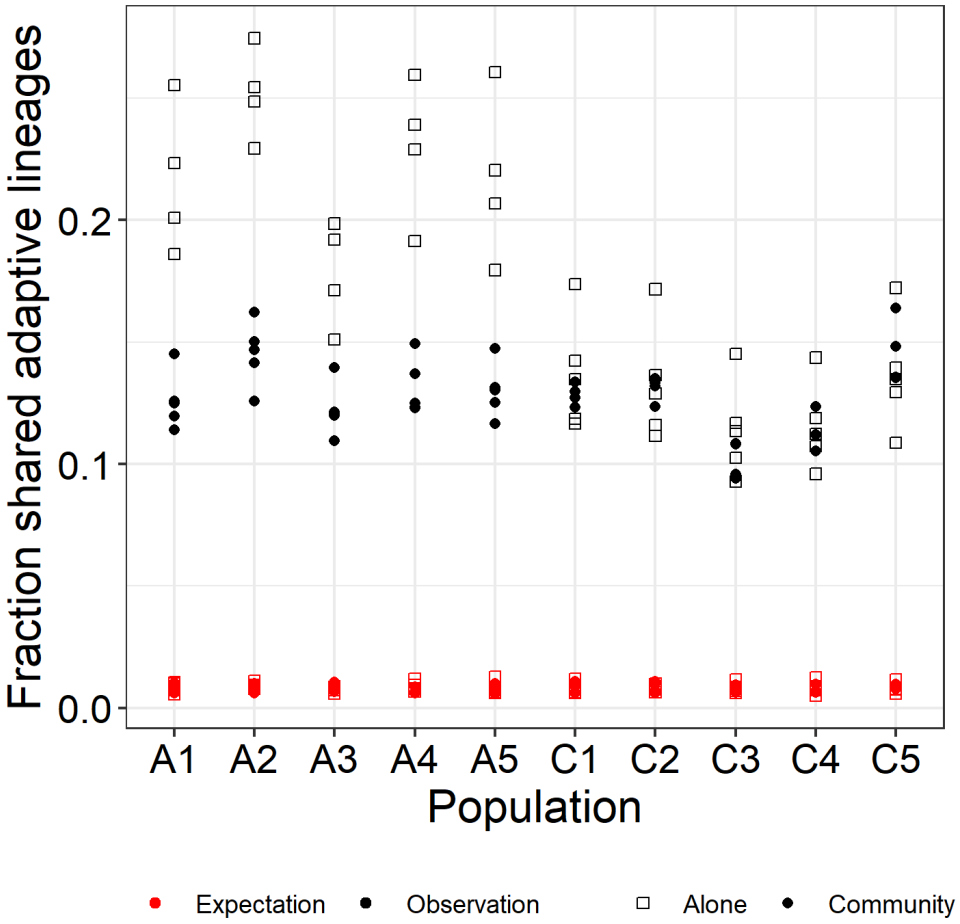

Figure S5. Evidence for pre-existing mutations in the BLT experiments. For each population on the x-axis, we plot the fraction of lineages identified as adapted in that population which are also identified as adapted in every other population (y-axis, black points) as well as the expectation for this fraction (red points). The expected overlap between populations i and j is calculated by comparing the observed adaptive lineages in population i to a random set of lineages from population j that reach detectable frequency. All lineages are considered equally for sampling.

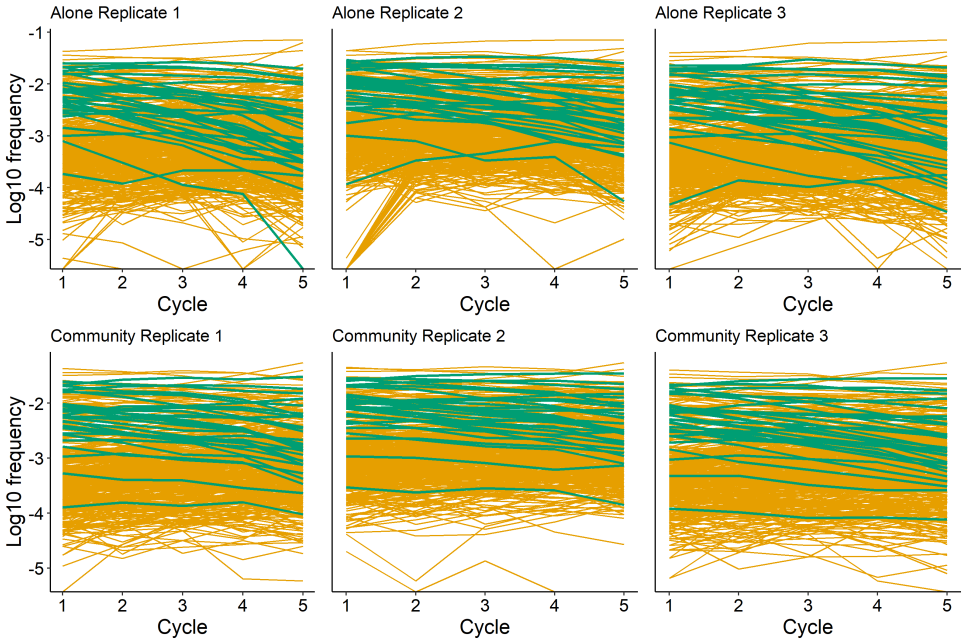

Figure S6. Lineage frequency trajectories in the competition assay. Reference lineages are shown in green, all other lineages are shown in orange.

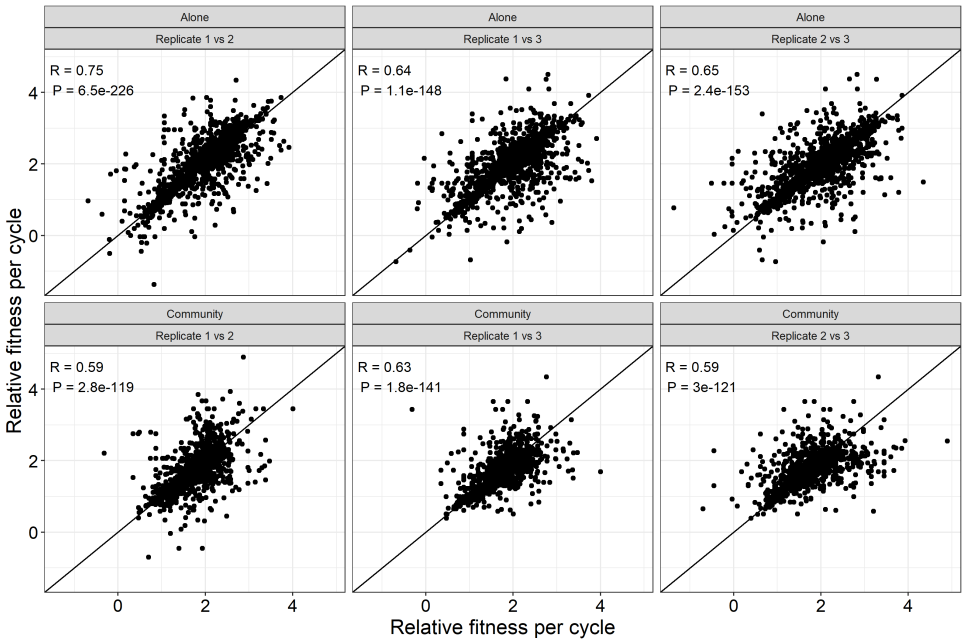

Figure S7. Correlation between fitness estimates across replicates of the competition assay. Line shows the diagonal.

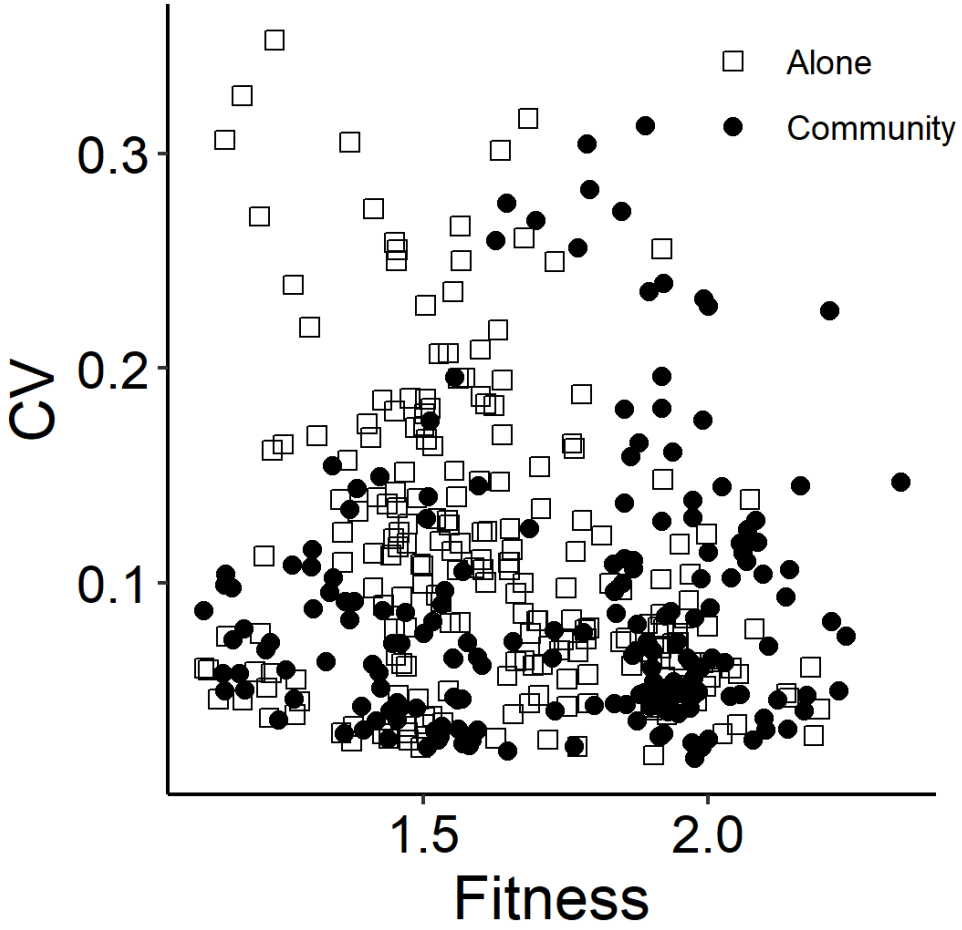

Figure S8. Mean and the coefficient of variation of the fitness estimates in the competition assay.

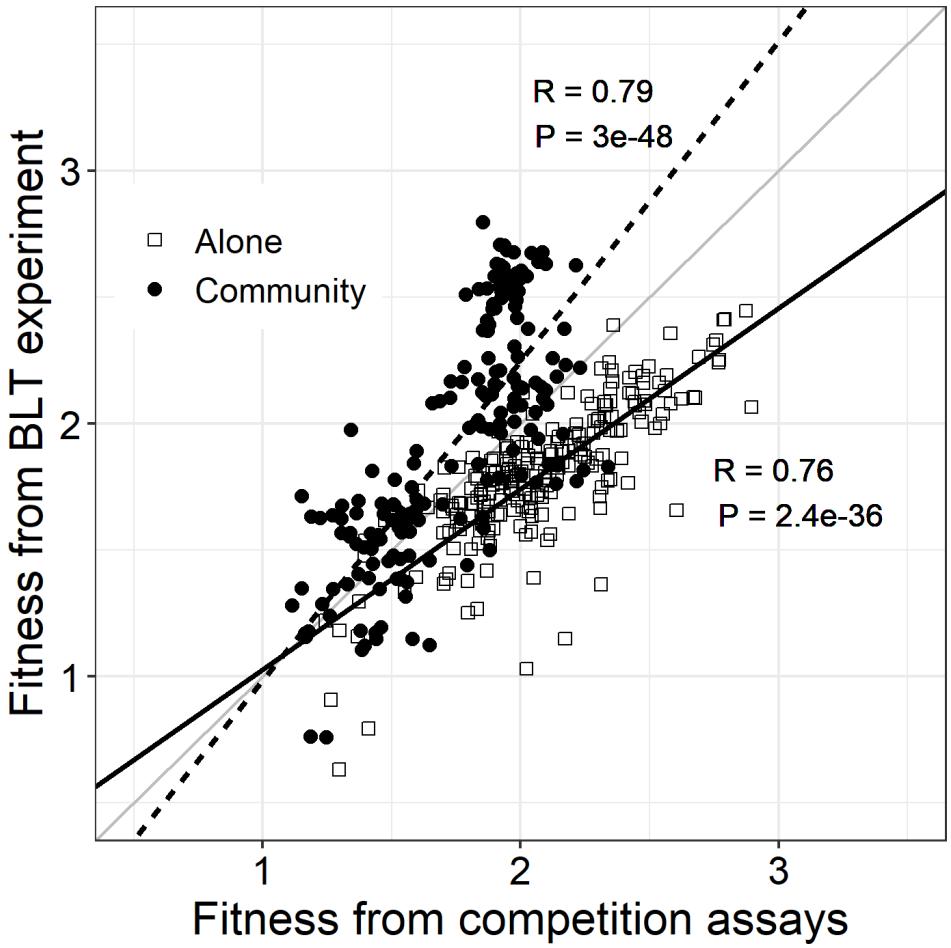

Figure S9. Correlation between BLT and competitive fitness estimates. Solid and dashed lines show linear regressions for the A-mutants (in the A-condition) and C-mutants (in the C-condition), respectively.

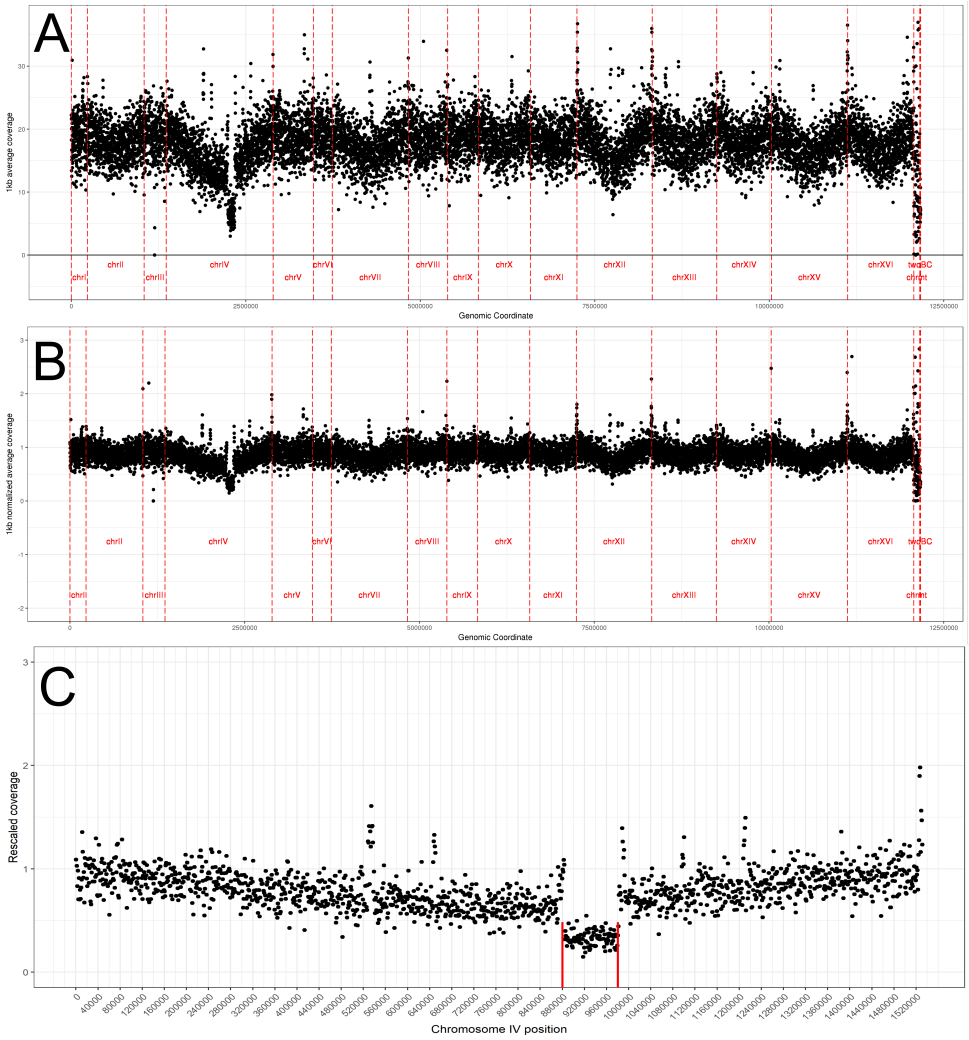

Figure S10. An example illustrating the detection of large chromosomal duplications and deletions in the genome sequence data. A. 1kb-window coverage plot for clone 386817 from population C1. **B.** Same data, after normalization using the relationship between coverage and chromosomal position shown in Figure S11. **C.** Focusing on chrIV to manually identify breakpoints for the chrIV-1n mutation (red lines).

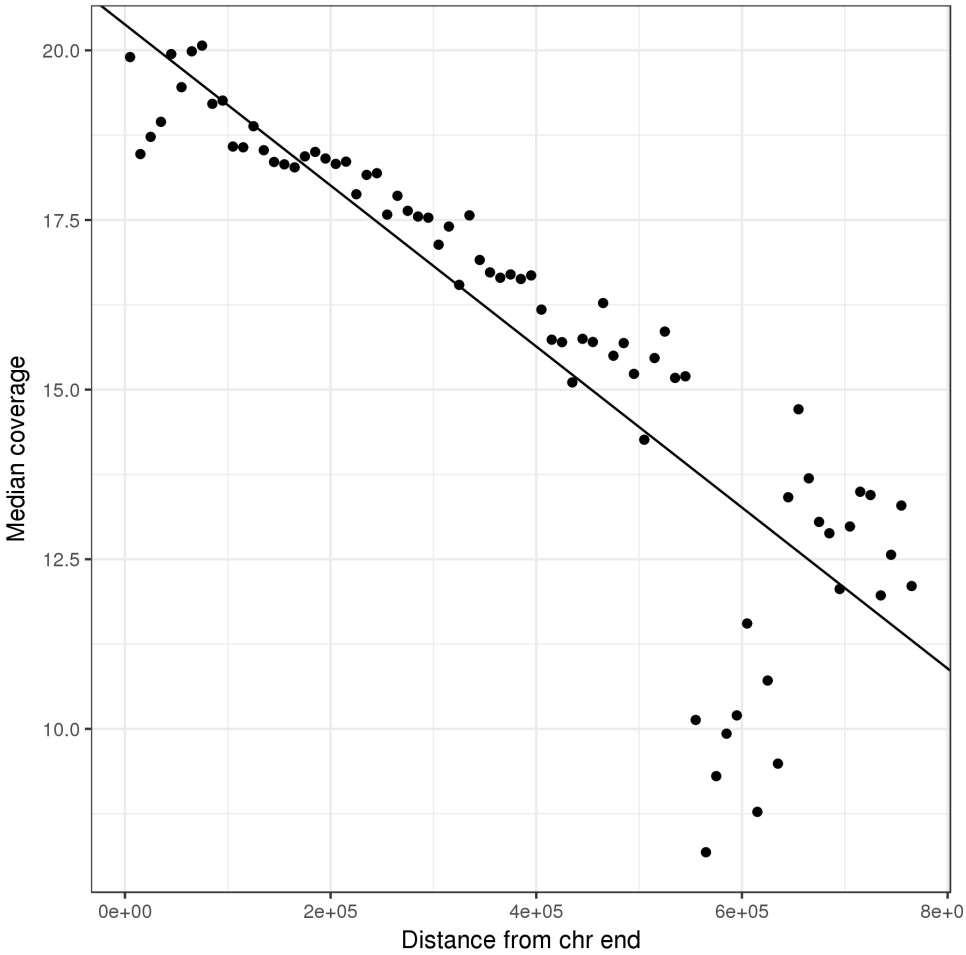

Figure S11. Relationship between coverage and chromosome position. Mean coverage in 1kb windows for clone 386817 from population C1 is shown vs distance of locus from the end of a chromosome.

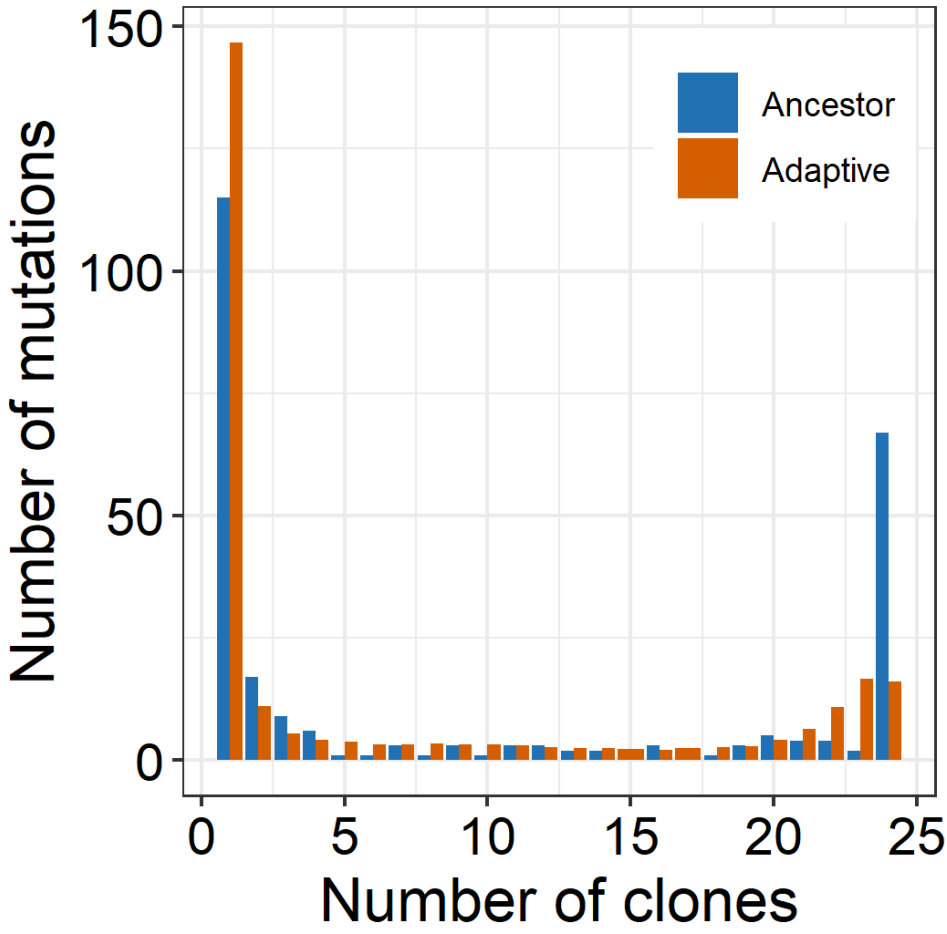

Figure S12. Allele frequency spectrum for ancestral and adapted isolates. Each bar shows the number of small mutations (point mutations and small indels) found in a given number of ancestral or adapted clones. The distribution for adapted clones is averaged over 1000 random draws of 24 clones.

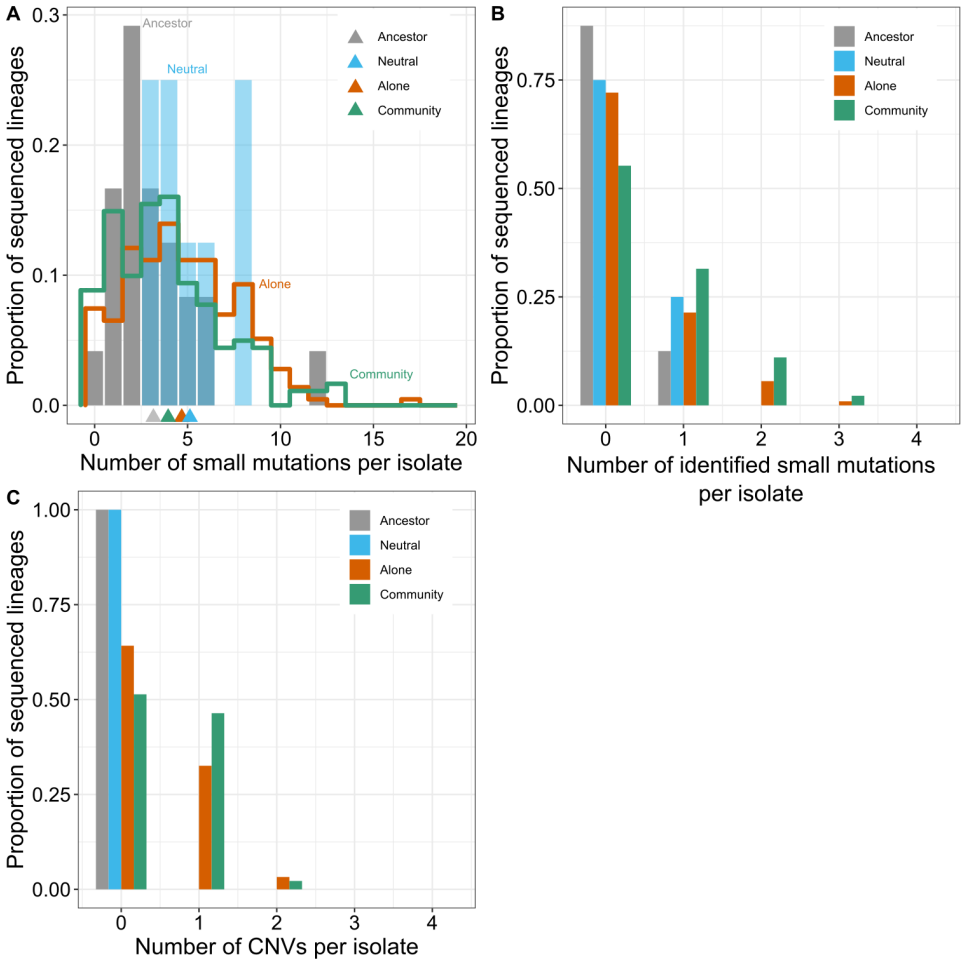

Figure S13. Distribution of mutations per clone. A. Number of small mutations detected per sequenced isolate. Triangles on the x-axis indicate the means of each distribution (see also Table S1). **B.** Distribution of the number of identified adaptive small mutations per isolate. **C.** Distribution of the number of CNVs per isolate.

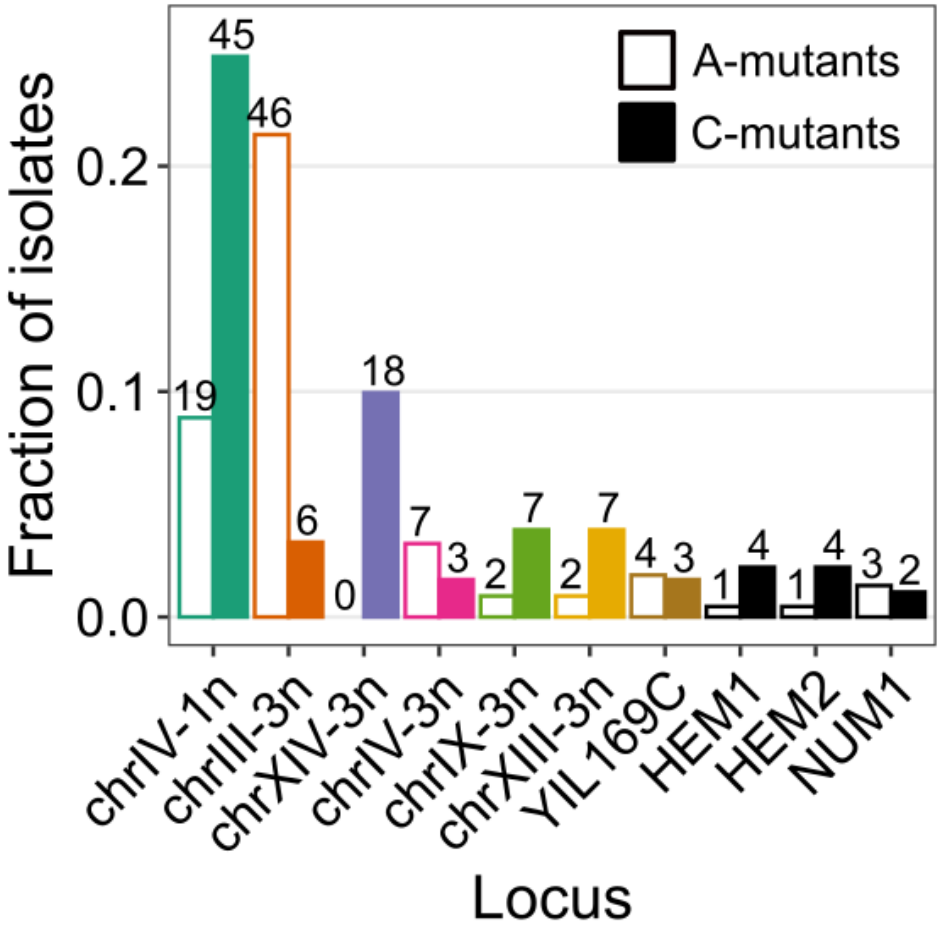

Figure S14. Distribution of adaptive mutations across the most common driver loci. Only driver loci with 5 or more mutations are shown (see Data S3 for the full distribution). Colors correspond to Figure 1 in the main text.

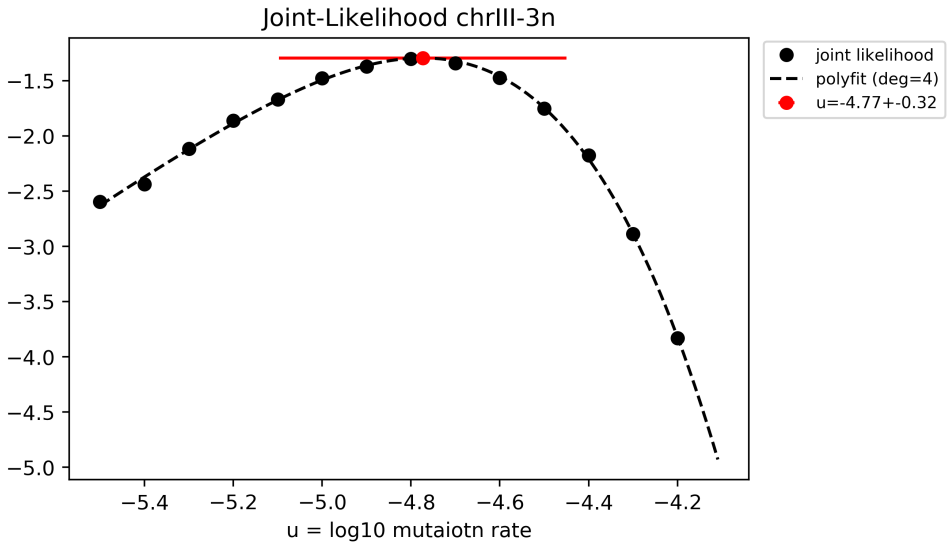

Figure S15. The log-likelihood function for the estimation of the chrIII-3n beneficial mutation rate.

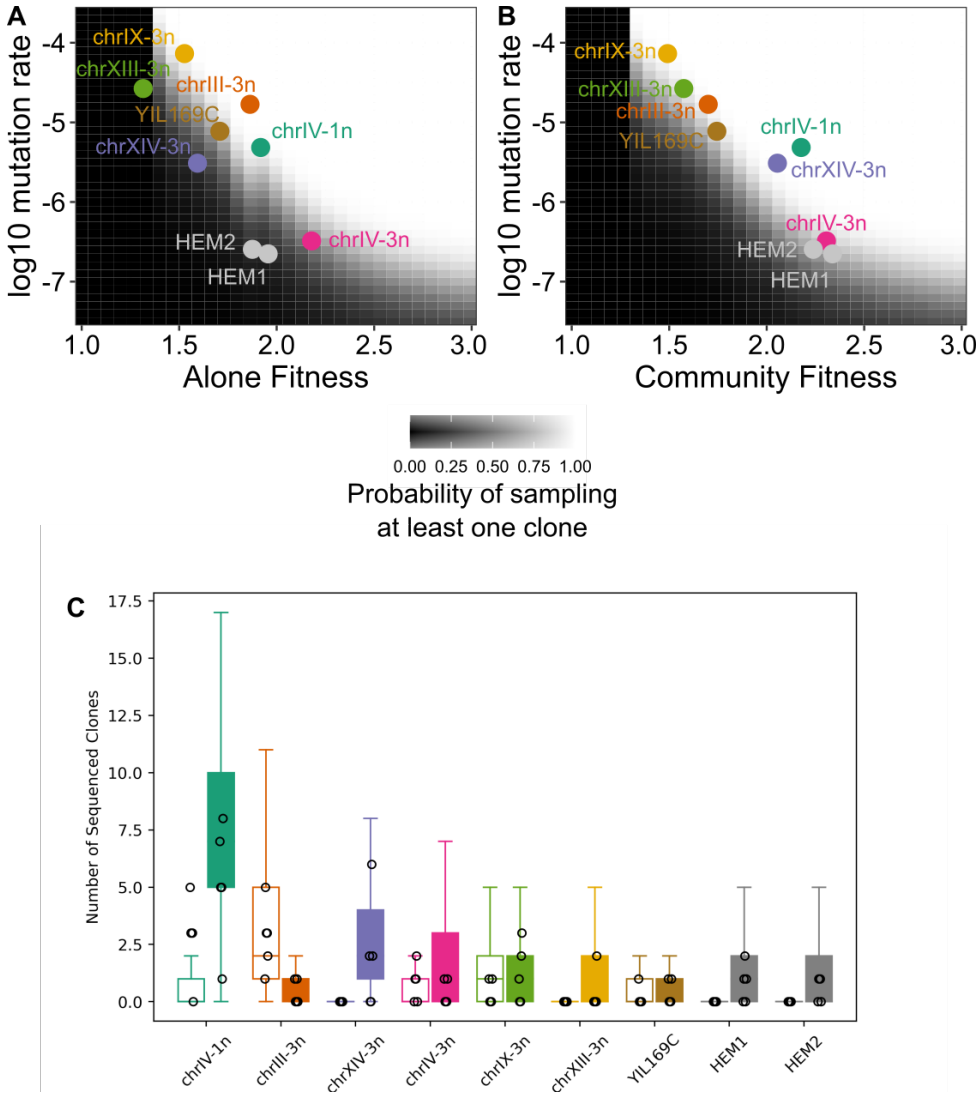

Figure S16. Sampling probabilities for adaptive mutations at the most common driver loci. A. Shades of gray show the probability of sampling at least one clone at a locus with a given beneficial mutation rate and fitness in the A-condition. The most common loci are shown by points with the same colors as in Figure 1 in the main text. The beneficial mutation rate and the selection coefficient for each mutation class are given in Table S2. **B.** Same as A but for the C-condition. The mutation rate for each locus is assumed to be the same in both conditions, but the selection coefficients vary. **C.** The observed number of sequenced clones per replicate population with a mutation in each class (black points) and the numbers expected in our simulations (bars and whiskers) given the measured selection coefficients and the estimated mutation rates provided in Table S2. Bars show IQR (Q3 − Q1), whiskers show Q1 − 1.5 × IQR and Q3 + 1.5 × IQR.

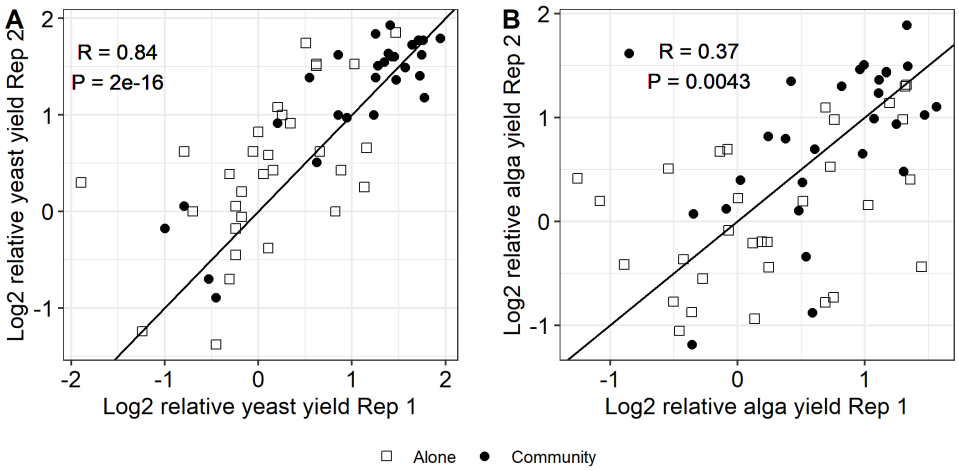

Figure S17. Correlation between yield measurements across replicates.

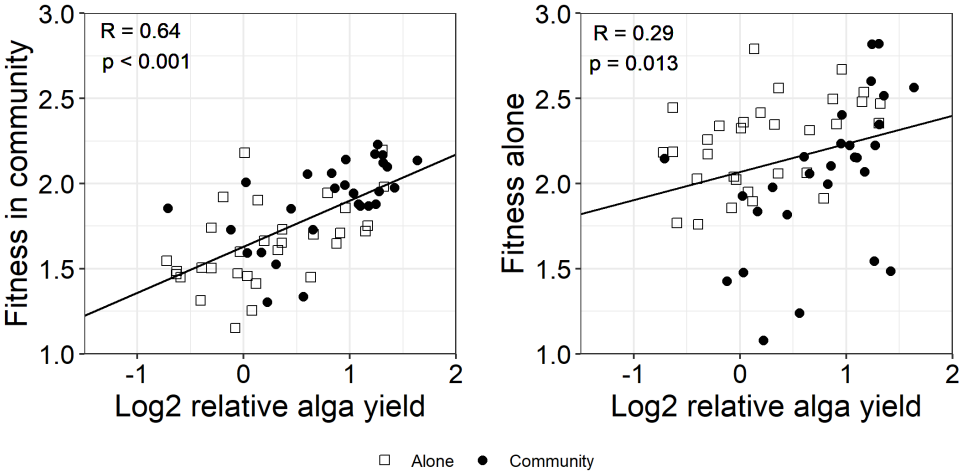

Figure S18. Correlation between yeast mutant fitness in the original community and alga yield in the mutant community.

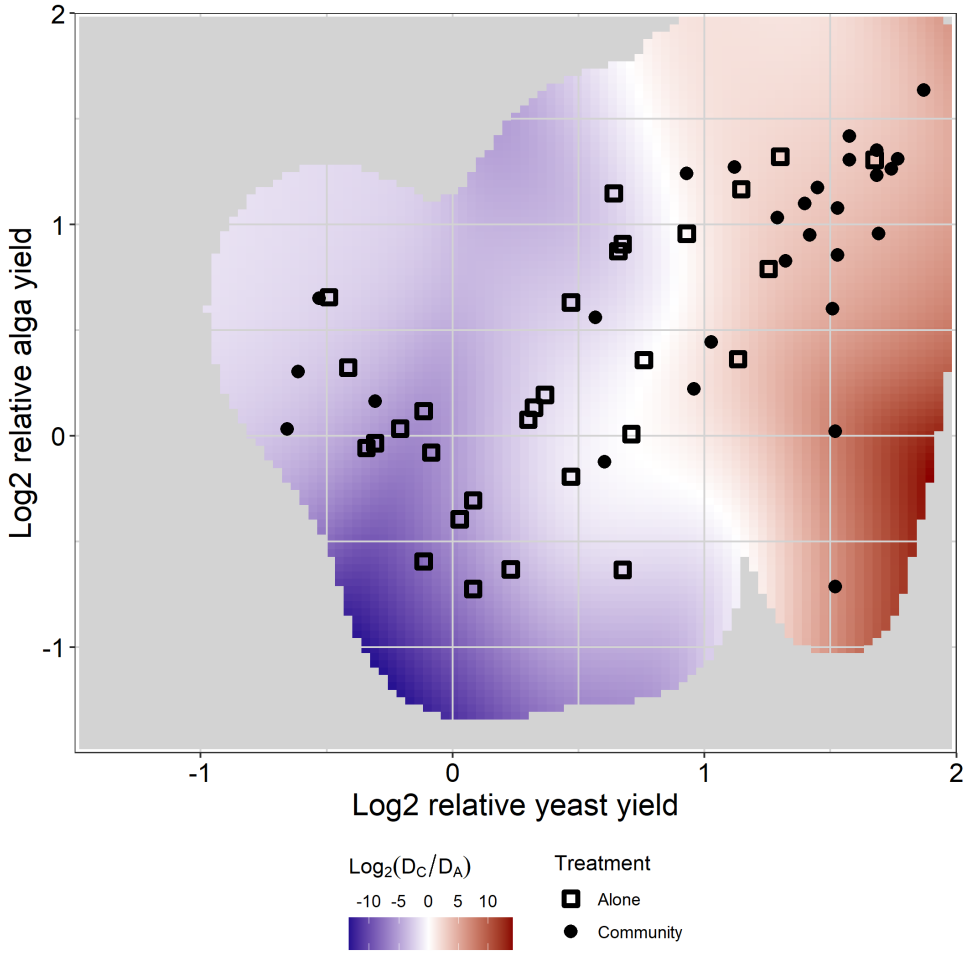

Figure S19. Estimated yeast and alga yields among random A- and C-mutants. The heatmap shows the ratio of probabilities of observing a given pair of yields among random C- and A-mutants. Data points are identical to Figure 2A in the main text. D_A and D_C were estimated from these data as described in Section 6.4. Any points where either D_A or D_C fall below 0.03 are colored gray.

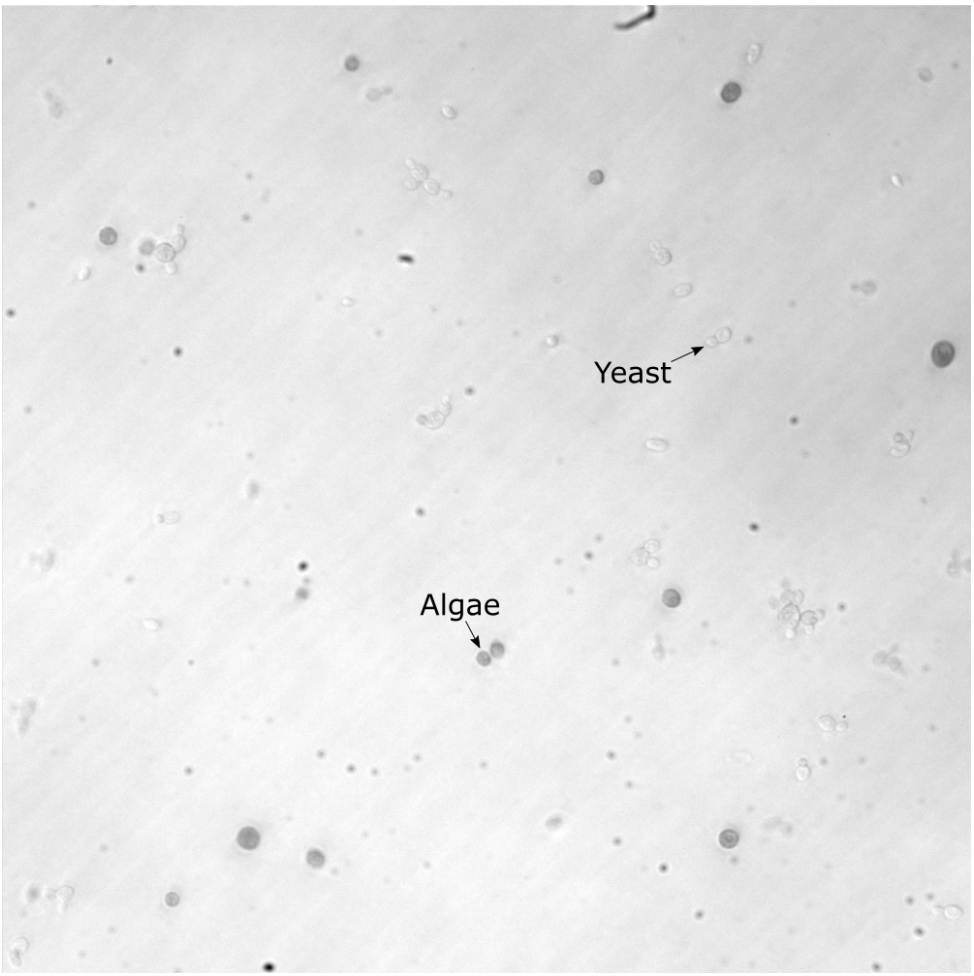

Figure S20. Representative microscopy image showing lack of physical associations between yeast and alga cells. Mutant culture formed by the C-mutant C2 109098 is shown. Some yeast and alga cells are indicated with arrows.

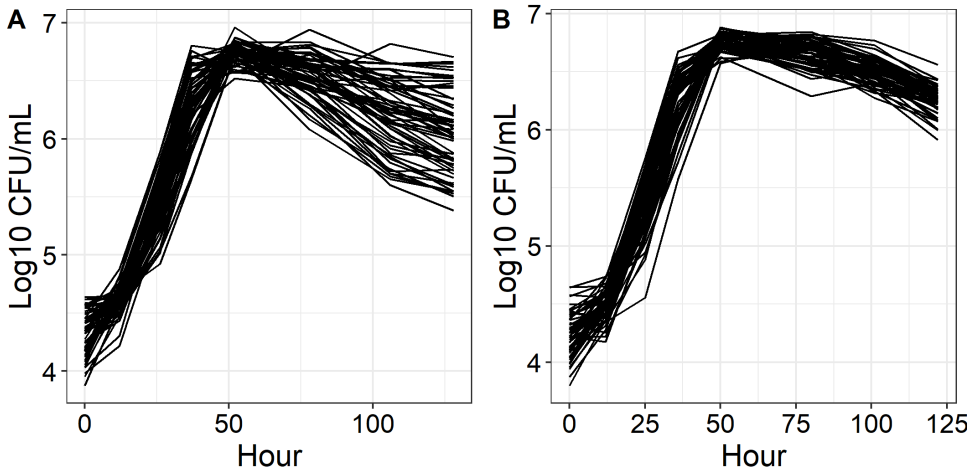

Figure S21. Mutant growth curves in the A-condition. Growth curves for the 59 adapted yeast mutants are shown, from which r and K values are estimated as described in Section 6.3. **A.** Replicate 1. **B.** Replicate 2.

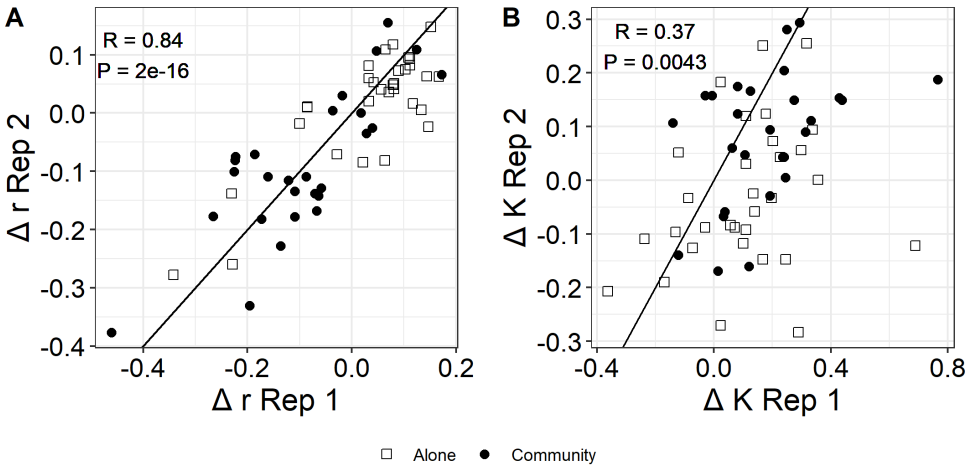

Figure S22. Correlation between replicates for r and K measurements.

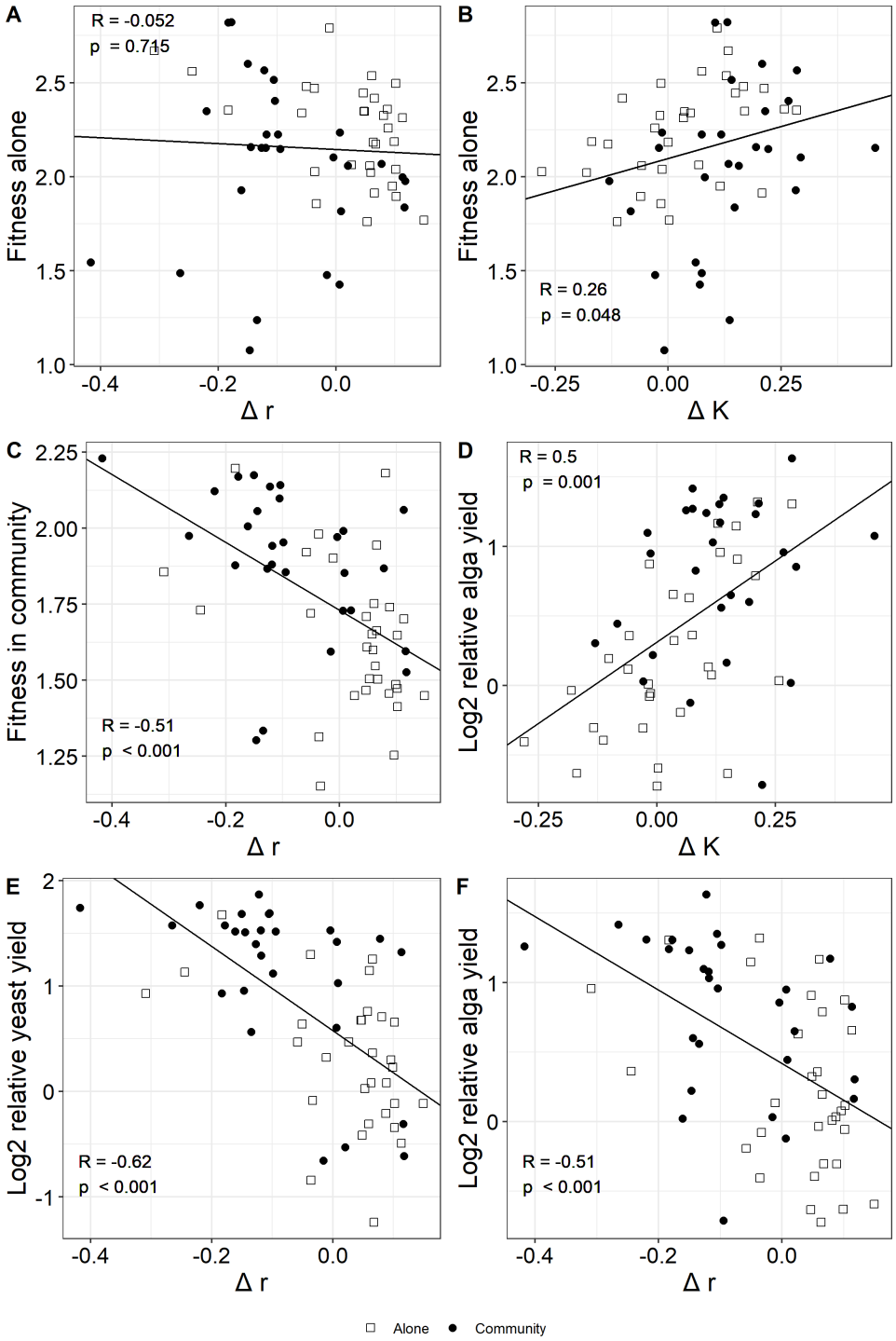

Figure S23. Relationship between growth parameters, yields and fitness. A. Δr vs fitness of mutants in the A-condition. **B.** ΔK vs fitness of mutants in the A-condition. **C.** Δr vs fitness in the C-condition. **D.** ΔK vs alga yield in mutant communities. **E.** Δr vs yeast yield in mutant communities. **F.** Δr vs alga yield in mutant communities.

9 Supplementary Tables

Isolates		Small variants				CNVs	
				Adaptive			
Type	Number	Total	Per isolate	Expected	Identified	Total	Per isolate
Ancestral	24	76	3.17 ± 0.51	–	3	0	–
Neutral	8	41	5.13 ± 0.72	–	2	0	–
A-mutants	215	1008	4.69 ± 0.20	$(0, 288)$	76	84	0.39 ± 0.04
C-mutants	181	717	3.96 ± 0.22	$(0, 110)$	109	92	0.51 ± 0.04
Total	428	1842	–	–	190	176	–

Table S1. Statistics of mutational counts among sequenced isolates

Culture	Seq. isolates	Mutation class m/Locus								
		chrIV-1n	chrIII-3n	chrXIV-3n	chrIV-3n	chrIX-3n	chrXIII-3n	YIL169C	HEM1	HEM2
A1	13	0	2	0	0	1	0	0	0	0
A2	17	3	3	0	2	0	0	0	0	0
A3	12	3	3	0	1	0	0	0	0	0
A4	19	3	5	0	1	0	0	0	0	0
A5	18	5	1	0	0	1	0	1	0	0
C1	25	8	0	2	1	3	2	1	1	0
C2	16	1	1	6	0	2	0	0	0	1
C3	21	5	0	0	0	0	0	0	2	1
C4	11	5	0	0	0	0	0	0	1	1
C5	24	6	1	2	1	1	0	1	0	0
	s_m^A	0.916	0.855	0.593	1.18	0.527	0.315	0.708	0.955	0.874
	s_m^C	1.17	0.689	1.05	1.3	0.492	0.575	0.744	1.34	1.24
	$\hat{u}_m$	-5.32	-4.77	-5.51	-6.49	-4.14	-4.58	-5.11	-6.65	-6.59

Table S2. Numbers of isolates carrying the most common adaptive mutations and the estimated mutation rates. Only clones with unique barcodes are shown. Column "Seq. isolates" shows the total number of sequenced isolates with unique barcodes sampled from each culture. Last row shows the estimated $u_m = \log_{10} U_m$.